Available online at www.sciencedirect.com
ScienceDirect
Geochimica et Cosmochimica Acta 71 (2007) 5913–5933
Geochimica et Cosmochimica Acta
www.elsevier.com/locate/gca

Adsorption and surface oxidation of Fe(II) on metal (hydr)oxides

Tjisse Hiemstra *, Willem H. van Riemsdijk

Department of Soil Quality, Wageningen University, P.O. Box 47, NL 6700 AA Wageningen, The Netherlands

Received 31 May 2007; accepted in revised form 18 September 2007; available online 12 October 2007

Abstract

The Fe(II) adsorption by non-ferric and ferric (hydr)oxides has been analyzed with surface complexation modeling. The CD model has been used to derive the interfacial distribution of charge. The fitted CD coefficients have been linked to the mechanism of adsorption. The Fe(II) adsorption is discussed for TiO_2, γ-AlOOH (boehmite), γ-FeOOH (lepidocrocite), α-FeOOH (goethite) and HFO (ferrihydrite) in relation to the surface structure and surface sites. One type of surface complex is formed at TiO_2 and γ-AlOOH, i.e. a surface-coordinated Fe^{2+} ion. At the TiO_2 (Degussa) surface, the Fe^{2+} ion is probably bound as a quattro-dentate surface complex. The CD value of Fe^{2+} adsorbed to γ-AlOOH points to the formation of a tridentate complex, which might be a double edge surface complex. The adsorption of Fe(II) to ferric (hydr)oxides differs. The charge distribution points to the transfer of electron charge from the adsorbed Fe(II) to the solid and the subsequent hydrolysis of the ligands that coordinate to the adsorbed ion, formerly present as Fe(II). Analysis shows that the hydrolysis corresponds to the hydrolysis of adsorbed Al(III) for γ-FeOOH and α-FeOOH. In both cases, an adsorbed $M(III)(OH)_2^+$ is found in agreement with structural considerations. For lepidocrocite, the experimental data point to a process with a complete surface oxidation while for goethite and also HFO, data can be explained assuming a combination of Fe(II) adsorption with and without electron transfer. Surface oxidation (electron transfer), leading to adsorbed $\equiv Fe(III)(OH)_2$, is favored at high pH ($pH > \sim 7.5$) promoting the deprotonation of two Fe_{III}-OH_2 ligands. For goethite, the interaction of Fe(II) with As(III) and *vice versa* has been modeled too. To explain Fe(II)–As(III) dual-sorbate systems, formation of a ternary type of surface complex is included, which is supposed to be a monodentate As(III) surface complex that interacts with an Fe(II) ion, resulting in a binuclear bidentate As(III) surface complex.

1. INTRODUCTION

Iron is an element that is dynamically present on the boundary between the oxidized and reduced world. Only a tiny shell of the geosphere is oxidized due to photosynthesis. On the long-term geo-historic record, it is a relatively recent phenomenon. Reduced conditions are maintained in water-logged soils and sediments due to back-consumption of oxygen and organic carbon by chemotrophic microorganisms. The rate of Fe(II) production by micro-organisms depends on the surface area of the ferric (hydr)oxide that is in contact with micro-organisms (Bonneville et al., 2006). Under intermediate redox conditions ($10 < pe < 0$) and neutral pH values, iron can be present as aqueous Fe(II) in combination with Fe(III) (hydr)oxides. Under these conditions, dissolved Fe(II) may interact with these ferric oxides and also with other minerals as well as organic matter.

Adsorbed Fe(II) is known to be very reactive (Stumm and Sulzberger, 1992), acting as a reductant for elements like Hg(II), As(V) (Charlet et al., 2002), U(VI) (Liger et al., 1999), Cr(VI) (Buerge and Hug, 1999) or Cu(II) (Maithreepala and Doong, 2004) and for the transformation or natural attenuation of organic components (Klausen et al., 1995; Liger et al., 1999; Amonette et al., 2000; Pecher et al., 2002; Vikesland and Valentine, 2002a,b; Strathmann and Stone, 2003; Klupinski et al., 2004; Maithreepala and Doong, 2004). In addition, adsorbed Fe(II) may strongly affect the Fe(III) dissolution rate of iron oxide minerals in the presence of organic anions (Stumm and Sulzberger, 1992; Ballesteros et al., 1998), and may catalyze

* Corresponding author. Fax: +31 317 419000.
E-mail address: tjisse.hiemstra@wur.nl (T. Hiemstra).

0016-7037/$ - see front matter © 2007 Elsevier Ltd. All rights reserved.
doi:10.1016/j.gca.2007.09.030

the transformation of Fe(III) minerals (Zhang et al., 1992; Hansel et al., 2005; Pedersen et al., 2005) In addition, adsorbed Fe^{2+} is far more easily oxydized if bound by mineral surfaces (Wehrli and Stumm, 1989; Wehrli et al., 1989).

Until recently, the interaction of Fe(II) with metal (hydr)oxides has only been studied sparingly under well-defined conditions. An important reason is the experimental challenge that is related to the work under reduced conditions, i.e. the oxidation rate of Fe(II) is very high in the experimental pH range of adsorption (Tamura et al., 1976; Emmenegger et al., 1998; King, 1998). Traces of oxygen will immediately lead to transformation of Fe(II) into Fe(III).

Unfortunately, a number of Fe (II) adsorption data have been collected in systems that are difficult to interpret unequivocally. Sometimes, the data refer to multi-component systems in which sulphate is present due to the addition of Fe(II) as Fe(II)SO_4 (Appelo et al., 2002; Charlet et al., 2002; Liger et al., 1999), or the systems contain simultaneously Ca^{2+} (Zachara et al., 2000) or bicarbonate (Choi et al., 2001). These ions may interfere. In other cases, combinations of ions have been chosen, like Fe(II) in $NaClO_4$ (Zachara et al., 2000; Vikesland and Valentine, 2002a) or Fe(II) in $NaNO_3$ (Liger et al., 1999; Appelo et al., 2002; Jeon et al., 2003) that are thermodynamically instable, although maybe not kinetically. We note that most Fe(II) adsorption data have been measured in NaCl solutions.

One of the most early adsorption data sets of Fe(II) is of (Zhang et al., 1992) who measured the Fe(II) adsorption on lepidocrocite (γ-FeOOH) in 0.6 M NaCl. Recently, (Nano and Strathmann, 2006) have measured the Fe(II) binding to TiO_2 and boehmite (γ-AlOOH) in NaCl and (Dixit and Hering, 2006) measured it recently for goethite (α-FeOOH). As will be discussed in this paper, interpretation of these data suggests that the Fe(II) adsorption behavior does not only depend on the types of surface sites that are involved in the binding, but that the Fe(II) binding may also depend on the presence of Fe(III) as component of the mineral structure. It has been suggested that in such a case an electron transfer between adsorbed Fe(II) and the mineral surface may occur (Williams and Scherer, 2004; Silvester et al., 2005; Larese-Casanova and Scherer, 2007). Electron transfer will lead to changes in the interfacial charge distribution, which may be detected by analyzing the Fe(II) adsorption phenomena with the charge distribution (CD) model (Hiemstra and van Riemsdijk, 1996a).

The CD model is a surface complexation model, in which the charge of a surface complex is not considered as single unit, but is assumed to be spatially distributed in the compact part of the interface. In the present study, we will apply the CD model to analyze the Fe(II) adsorption behavior and determine to what extent the resulting charge distribution can be related to surface oxidation of adsorbed Fe(II), or not. First, the adsorption of Fe(II) on non-ferric metal (hydr)oxides will be analyzed, i.e. TiO_2 and γ-AlOOH (boehmite). It will be compared with the situation for iron (hydr)oxides, in particular goethite, lepidocrocite and HFO. Before doing this, we will briefly discuss in the next section the factors that determine the interfacial charge distribution and we will introduce a recently suggested double layer picture (Hiemstra and van Riemsdijk, 2006) that has been used in the present data analysis.

2. THEORY

The complexity of the molecular processes on the microscopic level is studied with many advanced approaches, like spectroscopy and molecular modeling. The results of these studies can be useful for models that operate at the macroscopic scale. Surface complexation models are a good example. These models aim to describe the complexity of the macroscopic scale. To be successful, the molecular processes on the microscopic level are incorporated in a simplified manner. Below, two aspects will be elaborated on.

2.1. Interfacial charge distribution

In a double layer, the concept of point charges becomes problematic near the surface. Close to the surface, structural double layer details are needed. More than 80 years ago, Stern (1924) introduced the concept of charge separation between surface and counter ions to account for the minimum distance of approach of counter- and co-ions. Grahame (1947) extended the model, introducing electrolyte outer sphere complexation at the head end of the diffuse double layer, which was applied for the first time to metal oxide surfaces by Yates et al. (1974) and Davis et al. (1978a). In the first generation of surface complexation models, the charge of an innersphere surface complex has been condensed to a single unit that is located in the double layer profile. The location of ion charge in the electrostatic double layer is crucial in the modeling of the adsorption behavior of a component. This is due to the very large changes in the electrostatic potential in the inner compact part of the double layer (Hiemstra and van Riemsdijk, 2006). An innersphere complex experiences a gradient of electrostatic potentials. The corresponding electrostatic energy contribution cannot be calculated accurately with the simplified assumption of the presence of ion charge on one single electrostatic position in the interface. In the charge distribution model, one part of the charge of the innersphere complex is attributed to the surface. The remaining part is located at some distance from the surface.

A number of factors will determine the value of the interfacial charge distribution. First of all, the charge distribution will depend on the number of ligands that coordinate with the surface relative to the number of non-coordinating ligands. This has been demonstrated for a series of divalent oxyanions, comprising SO_4^{-2} and SeO_4^{-2}, MoO_4^{-2} and CrO_4^{-2}, and SeO_3^{-2} and CO_3^{-2} (Rietra et al., 1999a; Hiemstra et al., 2004). A refinement is necessary for ions that have a strongly asymmetrical coordination sphere. In that case, bond strength becomes an important parameter too. The bond strength is related to the relative bond length between the central ion of a complex and the coordinating ligands (Brown and Altermatt, 1985; Brown, 2002). In principle, the variation in bond length is experimentally accessible and can also be approached with molecular orbital (MO) calculations (Hiemstra and van Riemsdijk, 2006; Stachowicz et al., 2006;

Hiemstra et al., 2007; Rahnemaie et al., 2007). The variation in bond strength, due to differences in the geometry of metal surface complexes, can rationalize the differences in the CD values found for a series of divalent metal cations like Hg(II), Pb(II), Cu(II) and Cd(II) (Hiemstra and van Riemsdijk, 2002). Recently, a third point has come into focus. It has been suggested that the overall CD value is also affected by changes in the orientation of the water dipoles in the compact part of the double layer due the introduction of surface charge (Hiemstra and van Riemsdijk, 2006). The dipole orientation of water can partly reduce the electrostatic effect of the interfacial accumulation of charge. The dipole contribution is generally relatively small ($\sim$<0.15 valence units) but nevertheless often significant as has been shown for the adsorption of for instance uncharged $As(OH)_3$ (Stachowicz et al., 2006) and H_4SiO_4 (Hiemstra et al., 2007).

Finally, a new aspect is the possible change of the charge distribution in a surface complex due to electron transfer. If an adsorbed Fe(II) will release an electron that is taken up by an ion in the solid, the redistributed charge is a combination of the location of the electron in the surface and the adsorption of iron as Fe(III). Since Fe(III) is known for its strong hydrolysis, the electron transfer will also lead to release of protons from the water ligands that are bound to the adsorbed ion, formerly present as Fe(II).

2.2. Extended stern layer model

Recently, the interfacial double layer model has been refined (Hiemstra and van Riemsdijk, 2006) based on the analysis of titration data. Data were collected for goethite in a variety of electrolyte solutions containing Li^+, Na^+, K^+, Cs^+, -chloride or -nitrate (Rahnemaie et al., 2006). The experimental curves were internally consistent because of the use of a common stock suspension. Data analysis indicated that the head end of the diffuse double layer (DDL) was separated from the minimum distance of approach of electrolyte ions (ions pairs) by a second Stern layer (Hiemstra and van Riemsdijk, 2006). The double layer picture can be classified as an Extended Stern (ES) layer model (Westall and Hohl, 1980). As discussed in Hiemstra and van Riemsdijk (2006), the double layer structure that emerges can be explained by the alignment of water molecules near the surface in several layers, in which the electrolyte ions can only change stepwise their position. This picture agrees with experimental information obtained by different valuable approaches like force measurements (Pashley and Israelachvili, 1984; Israelachvili and Wennerstrom, 1996), X-ray reflectivity (Toney et al., 1995; Fenter and Sturchio, 2004; Catalano et al., 2006) and Sum Frequency Spectroscopy (Yeganeh et al., 1999; Kataoka et al., 2004; Ostroverkhov et al., 2005; Shen and Ostroverkhov, 2006). These measurements show increase in the ordering of water within a distance of about 0.7–0.9 nm, which is equivalent to about 2–3 layers of water molecules (Hiemstra and van Riemsdijk, 2006).

Sum Frequency Spectroscopy for silica, quartz, Al_2O_3(s), and TiO_2(s) (Shen and Ostroverkhov, 2006) shows that the number and orientation of polar water molecules changes with the interface charge (Yeganeh et al., 1999; Ostroverkhov et al., 2005). In case of the introduction of charge at the surface due to ion adsorption, water dipoles will orient in the electrostatic field. It results in a redistribution of charge in the compact part of the double layer, diminishing the induced field. The dipole orientation of the first water layer is implicitly part of the CD model as an approximation (Hiemstra and van Riemsdijk, 2006). The approximation has been quantified for use in the CD model and the dipole correction can be combined with the ionic charge distribution. This will be illustrated later in the text.

2.3. Calculations

The modeling and objective optimization of the adsorption parameters has been done using the ECOSAT 4.8 program (Keizer and van Riemsdijk, 1998) in combination with a recent version (2.581) of the program FIT of Kinniburgh (1993).

3. RESULTS AND DISCUSSION

In the following sections, we will discuss the adsorption of Fe(II) for a series of materials. We will compare the adsorption of Fe(II) on ferric and non-ferric (hydr)oxides. For each mineral, first the structure of the surface will be analyzed, including a brief discussion on the development of the primary charge. Next, we will discuss the possible geometry of the Fe(II) surface complex based on EXAFS information measured for the adsorption of other metal ions as far as available. The interfacial CD will be derived by modeling the Fe(II) adsorption and a mechanistic interpretation of the CD will be given. In the approach, the extended Stern layer model has been simplified by using equal values for the inner and outer Stern layer capacitance. This simplification has also been proposed by Sverjensky (2005).

3.1. TiO_2

3.1.1. Surface structure

In the mineral structure of TiO_2, e.g. rutile and anatase, all oxygen ions are triply coordinated. At the surface, one or two Ti ions are lacking leading to the formation of respectively doubly ($\equiv Ti_2O^{-2/3}$) and singly ($\equiv TiOH^{-1/3}$) coordinated surface groups. The charge attribution to these surface groups can be done using the bond valence concept of Pauling (1929). The Ti^{4+} ion is hexa-coordinated and neutralizes on average +2/3 valence units (v.u.) per bond. In the interior, three bonds with +2/3 v.u. are required to neutralize the negative oxygen charge ($z = -2$ v.u) leading to $\#Ti_3O^0$. A lower coordination of the oxygens at the surface will result in negative charge on these oxygens, which can be compensated by the adsorption of one or two additional protons per oxygen (Hiemstra et al., 1989a, 1996b). This leads to the definition of two proton adsorption reactions that can describe the surface charging behavior (Hiemstra et al., 1989b; Rodriguez et al., 1996; Machesky et al., 1998; Regazzoni et al., 1998; Bourikas et al., 2001; Ridley et al., 2004; Fitts et al., 2005; Jing et al., 2005):

$$\equiv TiOH^{-1/3} + H^+(aq) \iff \equiv TiOH_2^{+2/3} \quad (1)$$

and

$$\equiv Ti_2O^{-2/3} + H^+(aq) \iff \equiv Ti_2OH^{+1/3} \quad (2)$$

The proton affinity ($\log K_H$) of both types of surface groups can be estimated by calculating the potential degree of saturation of the oxygens charge by applying the Brown bond valence concept (Brown, 2002) in which the bond valence is linked to the Ti–O bond length. The estimated affinity constants explain the experimental PZC (Hiemstra et al., 1996b; Machesky et al., 2001) and also explain semi-quantitatively the in-situ IR absorption behavior observed by (Connor et al., 1999a) as discussed in Hiemstra and van Riemsdijk (2002).

3.1.2. Surface charge

The charging behavior of rutile and anatase has been evaluated by Bourikas et al. (2001), resulting in a set of recommended ion pair formation constants (Table 1). For reasons of simplicity, the proton affinity constants ($\log K_H$) of the above protonation reactions were set equal to the value of the PZC in the approach. Bourikas et al. (2001) reported that TiO_2 materials can be divided into two groups, i.e. those with a low Stern layer capacitance ($C \approx 0.9$ F/m^2), and those that have a higher capacitance ($C \approx 1.6$ F/m^2). The difference was attributed to the presence of a difference in hydration. However recently, it has been shown by spectroscopy that at the 1 1 0 face of rutile (Zhang et al., 2004), cations may coordinate to surface groups forming quattro-dentate complexes. This is not only observed for a variety of divalent and trivalent ions, but it was also found for Rb^+ at very high pH and concentration. Additional innersphere complexation of such cations will strongly increase the proton desorption, which will apparently lead to a higher value for the Stern layer capacitance if formation of such complexes is not taken into account. It can be shown that if formation of innersphere complexes for simple monovalent electrolyte ions is allowed in the analysis of the charging behavior, the capacitance value decreases to values that can be considered as more representative for the capacitance of the inner layer Stern layer, found for many well-crystallized minerals like goethite, gibbsite, etc.

3.1.3. Fe(II) binding to TiO_2

The adsorption of Fe(II) by TiO_2 (Degussa P25) has been studied by Nano and Strathmann (2006). The adsorption data are shown in Fig. 1 as function of pH, electrolyte level, and mineral loading of the system. Data have been modeled using the parameter set given in Table 1. In a first approach, we assumed the formation of a bidentate complex for adsorbed Fe^{2+}. This model approach leads to a fitted CD with a very high charge attribution to the surface plane ($\Delta z_0 \sim 1.4$ v.u.). The fitted charge distribution cannot be understood by the combination of the formation of a bidentate complex and a Pauling distribution of charge of Fe^{2+} over the coordinating ligands. If Fe^{2+} is hexa-coordinated, a charge of only 0.33 v.u. is attributed per bond. In case of a bidentate complex, the expected ionic surface charge attribution is only 0.67 v.u. This number strongly differs from the above fitted result ($\Delta z_0 \sim 1.4$ v.u.).

As mentioned in Section 3.1.2, it has been shown recently (Zhang et al., 2004) that a number of mono-, di- and trivalent metal ions may form quattro-dentate complexes at the 1 1 0 face of rutile (Fig. 2). If this molecular picture is valid for Fe(II) bound by TiO_2 (Degussa), we may write:

$$2\equiv Ti_2O^{-2/3} + 2\equiv TiOH^{-1/3} + Fe^{2+}(aq) \iff \equiv(Ti_2O)_2(TiOH)_2^{-2+\Delta z_0} - Fe(II)^{-\Delta z_1} \quad (3)$$

with $\Delta z_0 + \Delta z_1 = +2$ v.u. Application of this reaction in the modeling, results in a fitted interfacial CD value of $\Delta z_0 = 1.42 \pm 0.03$ v.u. and $\Delta z_1 = 0.58 \pm 0.03$ v.u. (Table 1). The calculated model lines are given in Fig. 1.

The fitted CD is now much more in agreement with a structural interpretation (Fig. 2). In case of a coordination of Fe(II) with four surface groups, assuming hexa-coordination, 4/6 of the ion charge ($n_0 = 1.33$ v.u.) will contribute to the neutralization of the common ligands in the surface.

Table 1
The location of ion charge (Extended Stern layer model) and affinity constants used to describe the experimental charging behavior of TiO_2 (Degussa) and the adsorption of Fe(II) with the CD model

Surface group[a]	Δz_0	Δz_1	Δz_2	$\log K$
$\equiv TiOH^{-1/3}$	0	0	0	0
$\equiv TiOH_2^{+2/3}$	1	0	0	6.3[b]
$\equiv TiOH^{-1/3}$–Na^+	0	1	0	−0.6[c]
$\equiv TiOH_2^{+2/3}$–Cl^-	1	−1	0	6.3 − 1.2 = 5.1[c]
$\equiv Ti_2O^{-2/3}$	0	0	0	0
$\equiv Ti_2OH^{+1/3}$	1	0	0	6.3[b]
$\equiv Ti_2O^{-2/3}$–Na^+	0	1	0	−0.6[c]
$\equiv Ti_2OH^{+1/3}$–Cl^-	1	−1	0	6.3 − 1.2 = 5.1[c]
$\equiv(TiO)_2(TiOH)_2$–Fe(II)	1.43 ± 0.03	0.57 ± 0.03	0	3.39[d] ± 0.03

The capacitance of the inner Stern layer is set equal to the value of the outer layer $C_1 \equiv C_2$. For TiO_2 (Degussa), a value of 0.9 F/m^2 (Bourikas et al., 2001) has been used.

[a] Sites density is set at 6 nm^{-2} for each group (Bourikas et al., 2001; Hiemstra et al., 1996b).

[b] Based on the PZC of TiO_2 of Degussa.

[c] From Bourikas et al. (2001).

[d] Fitted, this study.

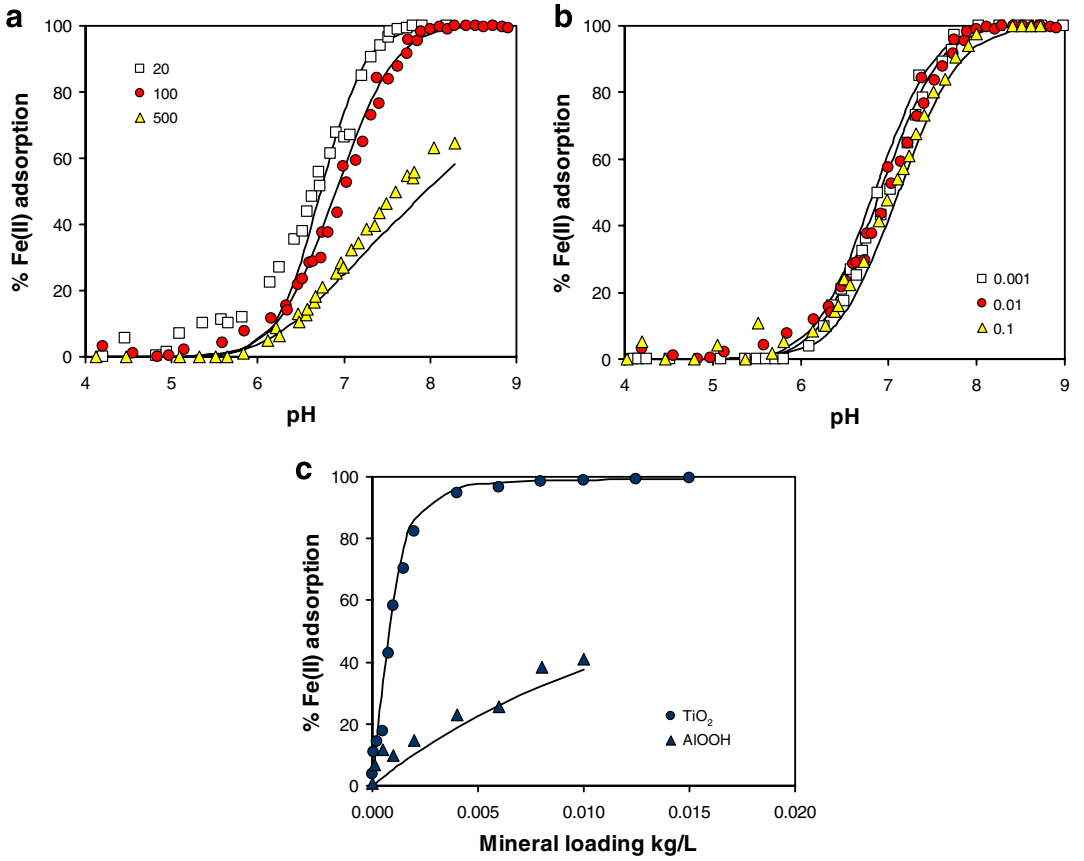

Fig. 1. (a) The adsorption of Fe(II) on TiO_2–Degussa (2 g/l, 50 m^2/g) as function of pH at three Fe(II) loadings (μmol/L) in 0.01 M NaCl. (b) The adsorption of Fe(II) (C–ini = 0.1 mM) on TiO_2–Degussa (2 g/l, 50 m^2/g) in NaCl as function of the ionic strength. (c) The adsorption of Fe(II) (C–ini = 0.1 mM) on TiO_2–Degussa (50 m^2/g) and γ-AlOOH (85.8 m^2/g) at pH 7.5, $I = 0.01$ M NaCl as function of mineral loading of the system. All data points are of Nano and Strathmann (2006). The lines are calculated with the CD model using the parameter set of Table 1.

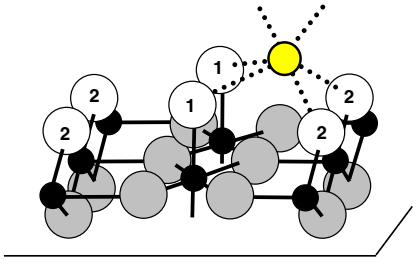

Fig. 2. The structure of the 110 face of rutile with in its interior oxygens (dark gray spheres) that are triply coordinated by Ti ions (small black spheres). At the surface, doubly and singly coordinated surface groups are present in rows (white spheres). A metal ion (light small sphere) may coordinate to two $\equiv Ti_2O^{-2/3}$ and two $\equiv TiOH^{-1/3}$ surface groups, resulting in a quattro-dentate complex.

The remaining part of the ion charge ($n_1 = 0.67$ v.u.), associated with the free ligands, is attributed to the first Stern plane.

As mentioned above, it has been proposed that the introduction of ion charge in the surface will result in a small redistribution due to dipole orientation of water molecules in the compact part of the double layer. It has been found that the dipole orientation will redistribute a charge ϕ of about 0.17 v.u. per unit of charge created in the surface plane. Formally, the correction term ($\phi\Lambda_0$) can be defined generally as (Hiemstra and van Riemsdijk, 2006):

$$\phi\Lambda_0 = \phi\left(n_0 + n_{H0} + \sum n_{ref} z_{ref}\right) \tag{4}$$

in which Λ_0 is the ionic charge introduced in the surface by the adsorption of metal ions (n_0) and any additional protons (n_{H0}), relative to the reference charge ($\sum n_{ref} z_{ref}$) that is found by the summation ($\sum$) of the charge on the reference groups (z_{ref}) over the number of reference groups (n_{ref}) as formulated in the reaction. Application of the equation to the Fe(II) adsorption on TiO_2 leads to $\phi\Lambda_0 = 0.17 * (1.33 + 0 + 2 * -2/3 + 2 * -1/3) = -0.11$ v.u. This correction term ($\phi\Lambda_0$) can be combined with the ionic charge distribution ($n_0 + n_{H0}$, $n_1 + n_{H1}$) that includes the ion charge and any additional protons, which have been formulated in the reaction. The combination results in the overall charge distribution coefficients (Δz_0, Δz_1):

$$\Delta z_0 = n_0 + n_{H0} - \phi\Lambda_0 \tag{5}$$

and

$$\Delta z_1 = n_1 + n_{H1} + \phi\Lambda_0 \tag{6}$$

In our case, application of these equations leads to the overall charge distribution coefficients $\Delta z_0 = n_0 - \phi \Lambda_0 = +1.33 + 0.11 = +1.44$ v.u. and $\Delta z_1 = n_1 + \phi \Lambda_0 = +0.67 - 0.11 = +0.56$ v.u. This number is, surprisingly or not, equal to the fitted value ($\Delta z_1 = 1.43$ v.u., $\Delta z_1 = 0.57$ v.u.) considering the uncertainty (±0.03 v.u.). We note that the agreement is only firm provided that the assumption of an equal distribution of the charge of adsorbed Fe(II) over its coordinating ligands is sufficiently valid. One may turn the reasoning, stating that apparently Fe(II) distributes its charge reasonably equal over the coordinating ligands.

The high charge attribution of an ion to the surface is equivalent with a strong pH dependency of the ion adsorption. A pH dependency can also be high due to the hydrolysis for the adsorbed species. Hydrolysis has been found upon adsorption of Zn^{2+} to rutile (Zhang et al., 2006). This ion can be bound in a monodentate fashion. Therefore, we have modeled the Fe^{2+}, assuming monodentate surface complex formation with in addition the possibility of hydrolysis. As constraint, we assumed the same charge attribution to the 0-surface plane for the binding of Fe^{2+} and $FeOH^{+}$, resulting in $\Delta z_0 = 0.34 \pm 0.02$ v.u. This number fully agrees with the CD value expected for a monodentate surface complex with hexa-coordination of Fe(II) ($\Delta z_0 = 0.33$ v.u.). However, we doubt the correctness of this picture because of the low value for the proton affinity constant of the adsorbed $FeOH^{+}$ species ($\log K_H = 6.7$) compared to the $\log K_H$ value for the hydrolysis in solution ($\log K_{H,Fe(OH)_2} = 11.1, \log K_{H,FeOH} = 9.5$). In case of Zn^{2+}, the enlarged hydrolysis is due to a decrease of the coordination number upon adsorption. A lower coordination number will increase the bond valence and therefore the neutralization of the ligands by the central ion which results in a lower proton affinity of the ligands. Change of the coordination number is less likely for Fe(II).

3.2. Boehmite (γ-AlOOH)

3.2.1. Surface structure

Boehmite (γ-AlOOH) is isostructural with lepidocrocite, the Fe analogue (γ-FeOOH) to be discussed later. In boehmite, two sheets of aluminum octahedra are linked together forming a bi-layer. In the interior of this layer, the oxygens are fourfold coordinated with respect to Al and at the exterior they are twofold coordinated. In the latter case, the oxygen is additionally neutralized by a proton forming the OH ion of γ-AlOOH. In the mineral, the layers are stacked in the *b*-axis direction and linked by hydrogen bonding.

Recently, the formation of γ-AlOOH has been studied in detail (Bokhimi et al., 2002). Well-crystallized boehmite, prepared with a sol gel method, forms rhombus-shaped thin flat crystallites (Fig. 3). It has been shown that the particles are bounded by the planar 010 face and at the edges by the 101 face and its equivalents. The size of the particles increases on aging, but the average shape is rather constant. Based on the average crystallite dimensions, one can calculate the ratio of the faces. The calculated surface area A of the both type of faces is $A_{face010}:A_{face101} \approx 2{:}1$.

We have analyzed the surface structure of the 010 face and the 101 faces. The 010 face is made up by surface OH groups that are doubly coordinated to Al^{3+} i.e. $\equiv Al_2OH^0$ with the deeper lying fourfold-coordinated oxygen ($\equiv Al_4O^0$). With respect to the $\equiv Al_2OH^0$ surface groups, the situation on the 010 face is partly comparable with the 001 face of gibbsite (Hiemstra et al., 1999b). At the 101 surface of boehmite, we have singly ($\equiv AlOH^{-1/2}$ or $\equiv AlOH_2^{+1/2}$ and doubly ($\equiv Al_2OH^0$) coordinated surface groups in a 1:1 ratio with a site density of $N_s = 6.8$ nm^{-2} for each type of surface group.

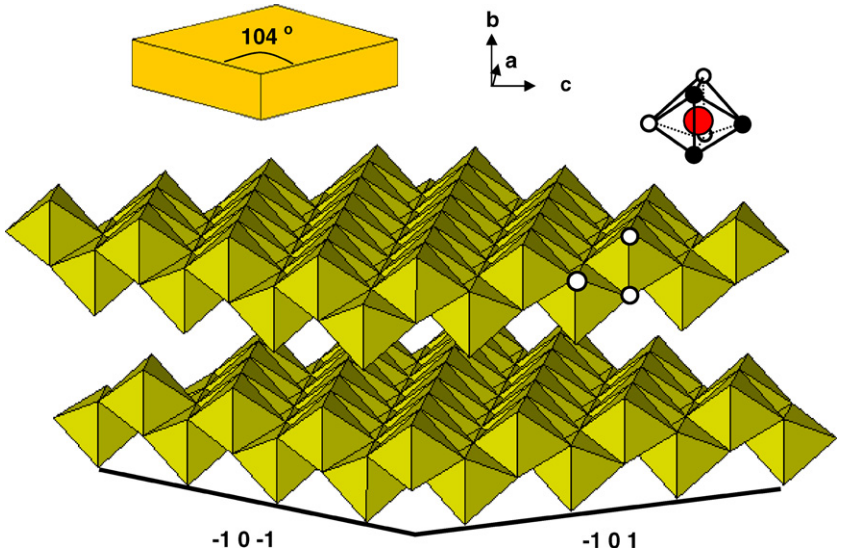

Fig. 3. The idealized morphology of sol–gel prepared crystallites of boehmite forming flat thin rhombuses, with the 010 face on top and bottom and at the edges the 101 face and its equivalents. The crystal structure is made up by sheets of AlOOH octahedra. On the top and bottom of each sheet, doubly coordinated OH groups are present. In the interior, fourfold-coordinated oxygens are found. The white spheres indicate the surface ligands (one singly and two doubly coordinated surface groups) involved in ion binding, resulting in double edge sharing.

3.2.2. Surface charge

The proton speciation of the surface groups (Table 2) has been estimated on the basis of the MUSIC model approach (Hiemstra et al., 1996b). As mentioned previously, the chemical affinity of a surface oxygen is related to the formal charge that is calculated using a bond valence approach. Part of the neutralization of the various surface oxygens is due to coordination with Al. Its contribution depends on the number of Al ions and the relative Al-O bond length. For boehmite, it has been found that the Al-O bond lengths in the Al coordination sphere depend on the crystallite size (Bokhimi et al., 2001). In small, nano-sized particles, the octahedron is more distorted. We have calculated the affinity constant for the surface protonation reactions of singly and doubly coordinated surface groups, using the experimental bond lengths reported by (Bokhimi et al., 2001) for the very small ($d_{020} \approx 1$–2 nm) and the large ($d_{020} \approx 10$–20 nm) particles. These particle sizes are equivalent with a calculated specific surface area (flat rhombuses) of respectively about 800 to 500 and 80 to 50 m^2/g. The results are summarized in Table 2. The proton affinities in Table 2 refer to the consecutive protonation reactions with, respectively, $\log K_{H1}$ and $\log K_{H2}$, formulated as:

$$\equiv AlO^{-3/2} + 2H^+(aq) \Longleftrightarrow \equiv AlOH^{-1/2} + H^+(aq) \Longleftrightarrow \equiv AlOH_2^{+1/2} \quad (7)$$

and

$$\equiv Al_2O^{-1} + 2H^+(aq) \Longleftrightarrow \equiv Al_2OH^0 + H^+(aq) \Longleftrightarrow \equiv Al_2OH_2^{+1} \quad (8)$$

For large 10–20 nm particles, the $\log K_{H1}$ for the protonation of $\equiv Al_2O^{-1}$ (Table 2) is very high. It implies that the doubly coordinated groups are very easily protonated to form $\equiv Al_2OH^0$. This surface species may accept a second proton but only at very low pH. It implies that a perfectly crystallized 0 1 0 face will usually have only $\equiv Al_2OH^0$ as surface group in the range of for instance pH 4–10. For very small nano-particles (“pseudo-boehmite”) a similar behavior is expected, but the formation of $\equiv Al_2O^{-1}$ may occur more easily at high pH, if the mineral is perfectly crystallized.

Table 2
The surface groups and corresponding calculated proton affinity constant affinity for the main crystal faces of boehmite

Face	Surface group	$\log K_H d \approx 1$–2 nm	$\log K_H d \approx 10$–20 nm
0 1 0	$\equiv Al_2O^{-1}$[a]	8.9	15.3
	$\equiv Al_2OH^{0}$[a]	−3.0	3.5
1 0 1	$\equiv AlO^{-3/2}$	18.3	21.7
	$\equiv AlOH^{-1/2}$	6.4	9.9
	$\equiv Al_2O^{-1}$	19.3	15.8
	$\equiv Al_2OH^{0}$	7.4	3.9

At the 0 1 0 face, the site density N_s is 9.75 nm^{-2} for the doubly coordinated surface groups. At the 1 0 1 face, the site density of the singly and doubly coordinated surface groups is both $N_s = 6.8$ nm^{-2}.

[a] In case of defects on the 0 1 0 face, singly and triply coordinated surface groups are created having a $\log K$ of respectively $\log K(\equiv AlOH) = 9.7$ and $\log K(\equiv Al_3O) = 5.3$.

The doubly coordinated surface OH groups at the 1 0 1 face of relatively large particles can also be considered as proton inactive in the given pH range. In contrast, the singly coordinated surface group is proton active. The $\equiv OH/OH_2$ groups will determine the surface charge and will suppress the reactivity of the doubly coordinated surface group as discussed in Hiemstra et al. (1989b). It can be shown that the $\log K_{H2}$ value of the singly coordinated surface group represents the pristine point of zero charge (PPZC). Depending on the particle size, the estimated value may vary between PPZC ≈ 6.4 and 9.9.

The charging behavior of boehmite has been measured by Nordin et al. (1997) and Klebanov et al. (2001) for particles with a surface area of respectively 180 m^2/g and 124 m^2/g. The reported PZC values are respectively about 8.6 and 8.5–8.8 (Klebanov et al., 2001). Within the uncertainties, these values are in reasonable agreement with the estimation for 10–20 nm particles if the singly coordinated surface groups at the 1 0 1 face determine the charging behavior.

The most extensive titration work for boehmite has been reported by Klebanov et al. (2001). According to the above analysis, a perfectly crystallized 0 1 0 face with only doubly coordinated surface groups is expected not to contribute significantly to the charging behavior in the normal pH range of titration. In the sol–gel preparation of Bokhimi et al. (2002), the 0 1 0 face represents about 67 ± 5% of total the surface area. If the development of surface charge is restricted to the edge faces, attribution of the experimental charge to only the 1 0 1 face will result in an unrealistically high surface charge. Therefore, we assume that the 0 1 0 face also contributes and that this is due to the presence of defects. In case of Al vacancies in the lattice on the 0 1 0 face, singly and triply coordinated surface groups are formed with respectively a $\log K_H$ of 9.6 and 5.3, which will lead to a PZC of approximately 7.5 if present in a 1:1 ratio. We have arbitrarily chosen an apparent site density for the triply and singly coordinated surface groups at a defect 0 1 0 face, i.e. $N_s(\equiv AlOH) = N_s(\equiv Al_3O) = 2$ nm^{-2}. This assumption leads to an estimated overall site density of $N_s(\equiv AlOH) = 3.6$ nm^{-2} and $N_s(\equiv Al_3O) = 1.3$ nm^{-2} for boehmite with a 1 0 1 face and 0 1 0 face contribution of respectively 1/3 and 2/3.

To describe the proton titration data, we used the ion pair formation constants previously determined for gibbsite (Hiemstra et al., 1999b), i.e. $\log K_{Na} = 0.2$ and $\log K_{Cl} = -0.2$ (Table 3). As simplification, the proton affinity of singly and triply coordinated surface groups is set equal and the $\log K_H$ is derived by fitting the charging leading to $\log K_H = 8.79 \pm 0.12$. The $\log K_H$ value represents the PPZC. The fitted Stern layer capacitance is $C_1 \equiv C_2 = 1.03 \pm 0.02$ F/m^2. For data of (Nordin et al., 1997) the capacitance was lower ($C_1 \equiv C_2 = 0.80$ F/m^2), which might point to a lower contribution of the 0 1 0 face to the overall charging behavior in that preparation.

3.2.3. Fe(II) adsorption to γ-AlOOH

So far, the formation of Fe(II) surface complexes on boehmite has not been studied spectroscopically. However, some information on ion complexation is available.

Table 3
Location of ion charge and affinity constants used to describe the experimental charging behavior (Klebanov et al., 2001) and the Fe(II) adsorption (Nano and Strathmann, 2006) of boehmite applying $C_1 = C_2 = 1.03$ F/m^2

Surface group	Δz_0	Δz_1	Δz_2	log$K$
$\equiv AlOH^{-1/2}$	0	0	0	0
$\equiv AlOH_2^{+1/2}$	1	0	0	8.79[a] ± 0.12
$\equiv AlOH^{-1/2}$–Na	0	1	0	+0.2[b]
$\equiv AlOH_2^{+1/2}$–Cl	1	−1	0	8.79 − 0.2[b] = 8.59
$\equiv Al_3O^{-1/2}$	0	0	0	0
$\equiv Al_3OH^{+1/2}$	1	0	0	8.79[a] ± 0.12
$\equiv Al_3O^{-1/2}$–Na	0	1	0	+0.2[b]
$\equiv Al_3OH^{+1/2}$–Cl	1	−1	0	8.79 − 0.2[b] = 8.59
$\equiv(Al_2OH)_2(AlOH)Fe_{II}$[c]	0.97 ± 0.05	1.03 ± 0.05	0	4.42[a] ± 0.02

[a] Fitted, this study.
[b] From Hiemstra et al. (1999b).
[c] The surface complex refers to edge sharing of Fe(II) with two Al octahedra.

Recently, the adsorption mode of another divalent metal ion, i.e. Ni^{2+}, has been measured with EXAFS (Strathmann and Myneni, 2005). Both metal ions have approximately the same ion size, i.e. ionic radius of Ni(II) = 68 pm and of Fe(II) = 73 pm (Marcus, 1983). In the first shell of the adsorbed Ni ion, six oxygens are found with a Ni-O bond length of 205 ± 1 pm. Two Al ions are found in the second shell at a distance of 298 pm. A structural interpretation of these distances is most consistent with edge sharing (Strathmann and Myneni, 2005). This finding can be used to identify for Ni(II) the adsorption site on the reactive surface of boehmite. According to data, two Al ions are present in the second coordination sphere. This can be interpreted as edge sharing of the Ni ion with two Al octahedra. According to Bokhimi et al. (2002), the morphology of well crystallized boehmite indicates that the 1 0 1 faces are chemically most reactive. Crystal growth at the 1 0 1 face can be seen as binding of Al ions at specific growth sites. The surface groups of this site are indicated in Fig. 3 with small white spheres. At crystal growth, edge sharing of the adsorbing ion with two Al octahedra of the solid will occur, resulting in an Al–Al distance of 287 pm. Based on the analogy sketched, we suggest that in case of Ni(II) and also Fe(II) adsorption, the same structural position is occupied.

An important question is the protonation status of the common ligands in case of the formation of a M(II) surface complex. If the common ligand would be an oxygen ion, it will become highly undersaturated with respect to charge. Using a bond valence approach, one calculates for the charge on the ligand in ≡Al–O–Ni and ≡Al_2–O–Ni bond respectively −1.13 v.u. and −0.67 v.u. if the Ni(II) ion contributes 0.33 v.u. and the Al ion(s) on average 0.5 v.u. (Pauling bond valences). The high degree of undersaturation suggests a high proton affinity, i.e. formation of an OH as common ligand is expected. In that case, the adsorption reaction of Fe(II) ions can be formulated as:

$$2{\equiv}Al_2OH^0 + 1{\equiv}AlOH^{-1/2} + Fe^{2+}(aq) \Longleftrightarrow {\equiv}(Al_2OH)_2(AlOH)^{-1/2+\Delta z_0}Fe_{II}^{\Delta z_1} \quad (9)$$

where $\Delta z_0 + \Delta z_1 = 2$. Application of this adsorption reaction in the modeling enables a good description ($R^2 = 0.96$) of the adsorption data (Figs. 1c and 4). Arbitrarily, the site density of the doubly coordinated surface groups has been set equal to that of the singly coordinated surface groups ($N_s = 3.6$ nm^{-2}). The precise value has a minor influence (about 0.05 v.u.) on the fitted CD value. The fitted CD value and log$K$ value are given in Table 3.

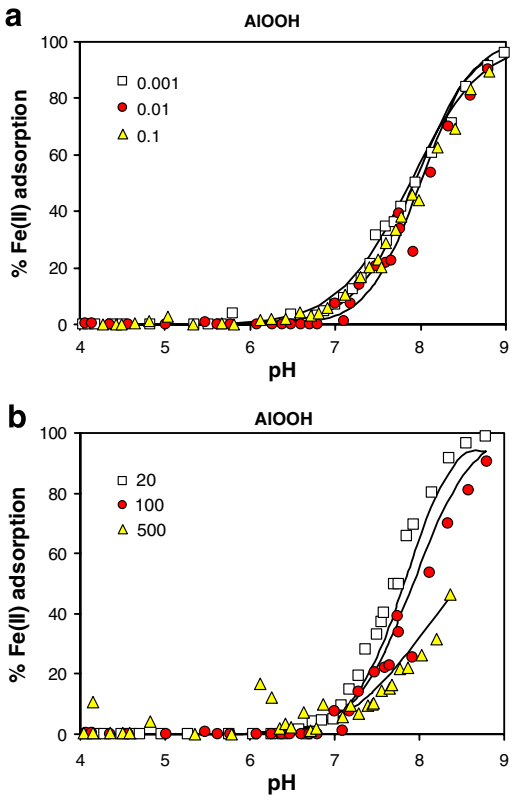

Fig. 4. (a) The adsorption of Fe(II) on boehmite (5 g/l, 85.6 m^2/g) as function of pH at three Fe(II) loadings (μmol/L) in 0.01 M NaCl. (b) The adsorption of Fe(II) (C–ini = 0.1 mM) on boehmite (5 g/l, 85.6 m^2/g) in NaCl as function of the ionic strength. Data points are of Nano and Strathmann (2006). The lines are calculated with the CD model using the parameter set of Table 3.

The fitted CD value can be interpreted structurally. In this approach, we assume that the adsorbed Fe(II) will distribute the charge equally over its ligands, i.e. equal Fe–O

distances. In case of coordination of a Fe(II) ion with three surface groups, assuming hexa-coordination, half of the ion charge will be attributed to the common ligands in the surface. The other half will be attributed to the free ligands in the Stern plane. It results in an ionic charge distribution coefficients of $n_0 = +1.0$ v.u. and $n_1 = +1.0$ v.u. Correcting for the dipole effect by applying Eqs. (4)–(6) ($\phi\Lambda_0 = 0.17 * (1 + 0 + 1 * - 1/2) \approx 0.09$ v.u.) results in the overall charge distribution coefficients $\Delta z_0 = n_0 - \phi\Lambda_0 = +0.91$ v.u. and $\Delta z_1 = n_1 + \phi\Lambda_0 = +1.09$ v.u. The above fitted CD values are in agreement with the calculated ones, which supports the proposed adsorption mechanism of the formation of a tridentate Fe(II) complex at the surface.

In summary, we conclude that the adsorption of the surface of TiO_2 and γ-AlOOH can be described as Fe(II) complexation without the assumption of any electron transfer. The differences in behavior of these two minerals phases can be linked satisfactory to a binding at particular sites.

3.3. Lepidocrocite γ-FeOOH

3.3.1. Surface structure

Lepidocrocite is isostructural with boehmite. Lepidocrocite (Fig. 5) may have a rod or a plate-like morphology (Lewis and Farmer, 1986; Manceau et al., 2000) or a combination in which the elongated plates finger out in rods in the crystallographic c-direction (Weidler, 1996). Main mineral faces are supposed to be the 0 1 0 and 100 faces. Manceau et al. (2000) showed that 1 0 1 faces may develop too. These crystal faces can be formed at the *c*-axis termination of elongated crystals as sketched in Fig. 5.

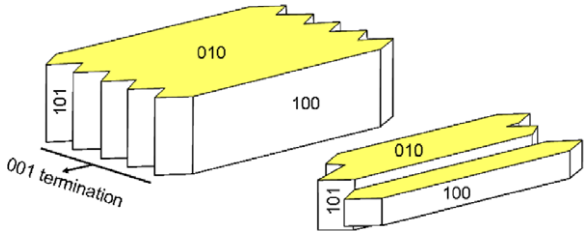

Fig. 5. The idealized and simplified morphology of lepidocrocite crystals, with the 0 1 0 face on top and bottom and at the edges the 100 face and at the termination in the *c* direction 1 0 1 faces can be formed.

Atomic force measurements showed a relative contribution of the 0 1 0 face of about 70% (Manceau et al., 2000) for plate-like particles.

The surface composition of the various faces is given in Table 4. As for boehmite, the surface groups at the 0 1 0 face of lepidocrocite are all doubly coordinated (≡Fe_2OH) if the 0 1 0 face is perfectly crystallized. The 100 face consists of three rows of singly (≡FeOH) and one row of triply (≡Fe_3O) coordinated surface groups (Manceau et al., 2000). At the 1 0 1 face and its equivalents, a combination of singly and doubly coordinated surface groups is found in a 1:1 ratio (Table 4).

3.3.2. Surface charge

The proton affinity of the various surface groups has been estimated with the MUSIC approach in which the potential saturation of the surface oxygen is calculated on the basis of the neutralization by Fe, protons and H bonds. For Fe, the bond valence is calculated based on the bond lengths, being 198, 201, or 207 pm (Zhukhlistov, 2001), giving a bond valence of, respectively, 0.55, 0.51 and 0.43 v.u. The proton is assumed to contribute 0.8 v.u. and a H-bond 0.2 v.u. The $\log K_H$ values for the consecutive protonation steps are given in Table 4. In case of a perfect crystal and perfect faces, the 1 0 1 and 100 can be considered as proton reactive with a PZC of respectively 9.7 and 7.3. As for boehmite, the main 0 1 0 face will not be reactive if it is perfectly crystallized. However, the experimental data for several materials (Madrid and Diazbarrientos, 1988; Venema et al., 1998; Zhang et al., 1992) indicate that we have to assume that these faces contribute considerably to the overall surface charge, similar as for boehmite. The singly and triply coordinated surface groups that are supposedly present have a proton affinity of respectively $\log K_{H2} = 9.7$ and $\log K_{H1} = 5.3$ which will lead to a PZC of approximately 7.5 if present in equal numbers.

The PZC values reported for various lepidocrocite preparations are approximately PZC = 7.2 (Davies and Morgan, 1989), PZC = 7.3 (Zhang et al., 1992), PZC = 7.7 (Peacock and Sherman, 2004), PZC = 8.0 (Venema et al., 1998; Madrid and Diazbarrientos, 1988).

Based on the above analysis, we make a simplification in order to make a representative description of the charging behavior. Assuming an apparent site density of 2 nm^{-2} for ≡FeOH and ≡Fe_3O at the defect 0 1 0 face and a

Table 4
The surface groups and corresponding predicted proton affinity constants affinity for the main crystal faces of lepidocrocite

Face	Reference surface group	N_s (nm^{-2})	$\log K_{H1}$	$\log K_{H2}$
0 1 0[a]	$\equiv Fe_2O_{II}^{-1}$ or $Fe_2O_{II}H^0$	8.4	11.5	−0.4
100	$\equiv FeO_I^{-3/2}$ or $\equiv FeO_IH^{-1/2}$	4.1	21.6	**9.7**
	$\equiv FeO_{II}^{-3/2}$ or $\equiv FeO_{II}H^{-1/2}$	8.2	23.1	11.3/**7.3**[b]
	$\equiv Fe_3O_I^{-1/2}$	4.1	**5.3**	–
101	$\equiv FeO_I^{-3/2}$ or $\equiv FeO_IH^{-1/2}$	6.5	21.6	**9.7**[c]
	$\equiv Fe_2O_{II}^{-1}$ or $\equiv Fe_2O_{II}H^0$	6.5	13.1	1.2

[a] In case of the presence of defects, singly and triply coordinated surface groups are found having a $\log K_H$ of respectively 9.7 and 5.3, resulting in a PZC of 7.5.
[b] The lower value is found if two H bonds are formed with this group resulting in a PZC = 7.3.
[c] The PZC of this face is expected to be high, i.e. PZC = 9.7.

Table 5
Location of ion charge and affinity constants used to describe the experimental charging behavior and Fe(II) adsorption of lepidocrocite of Zhang et al. (1992)

Surface group	Δz_0	Δz_1	Δz_2	log$K$
$\equiv FeOH^{-1/2}$	0	0	0	0
$\equiv FeOH_2^{+1/2}$	1	0	0	7.12 ± 0.1[a]
$\equiv FeOH^{-1/2}$–Na	0	1	0	-0.60[b]
$\equiv FeOH_2^{+1/2}$–Cl[c]	1	-1	0	7.12–0.45[b]
$\equiv FeOH_2^{+1/2}$–NO_3[c]	1	-1	0	7.12–0.70[b]
$\equiv(FeOH)_2$–$Al(OH)_2$[d]	$+0.86 \pm 0.05$	$+0.14 \pm 0.05$	0	-0.47 ± 0.09
$\equiv(FeOH)_2$–$Fe_{III}(OH)_2$[e]	$+0.24 \pm 0.10$	-0.24 ± 0.05	0	-6.96 ± 0.09

The fitted capacitance value is $C_1 = C_2 = 1.24 \pm 0.05$ F/m^2 (Extended Stern layer model).
[a] Fitted.
[b] From Rahnemaie et al. (2007).
[c] Cl in case of Zhang et al. (1992) and NO_3 in case of Silvester et al. (2005).
[d] Defined in Eq. (10).
[e] Defined in Eq. (11) as Fe^{2+} adsorption with interfacial electron transfer.

relative contribution of the 010, 100 and 101 faces of respectively 2/3, 1/6 and 1/6, the apparent site density is about 4 sites per nm^2 for the singly coordinated and 2 nm^{-2} for the triply coordinated surface groups. We further simplify by setting the logK_H value for both types of surface groups equal to the value of the PZC as done for TiO_2 and γ-AlOOH. For the ion pair formation constants, we rely on the values found for goethite (Rahnemaie et al., 2007).

Using this approach, we have modeled the surface charge behavior of (Madrid and Diazbarrientos, 1988; Zhang et al., 1992; Venema et al., 1998), resulting in a set of Stern layer capacitances ($C_1 = C_2$) of respectively 0.79, 1.24, and 0.98 F/m^2. The value of (Zhang et al., 1992) is rather high. Their material has a rather low surface area ($A_{BET} = 17.1$ m^2/g), in contrast to both other materials which have respectively $A_{BET} = 116$ m^2/g and 73 m^2/g. Increase of the apparent capacitance with decreasing surface area has previously also been noticed for goethite (Hiemstra et al., 1989b; Boily et al., 2001; Gaboriaud and Ehrhardt, 2003; Sverjensky, 2005). The parameters for the description of the proton adsorption data of Zhang et al. (1992) are given in Table 5. The proton titration curve in 0.6 M NaCl is shown in Fig. 6.

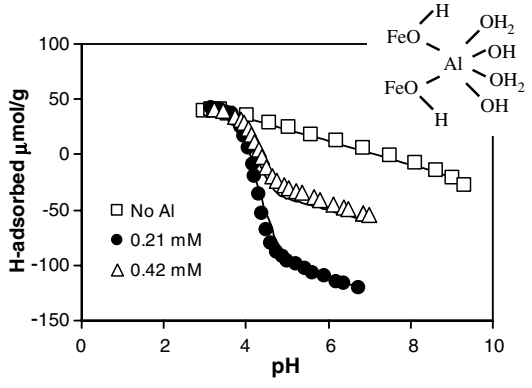

Fig. 6. The variation in the proton adsorption of lepidocrocite (10 g/l, 17.1 m^2/g) in the absence and presence of Al(III) as function of the pH ($I = 0.6$ M NaCl). Data are from Zhang et al. (1992). The lines have been calculated using Eq. (10) and Table 5.

3.3.3. Al^{3+} adsorption to γ-FeOOH

The adsorption of Fe(II) might be accompanied by the transfer of an electron, changing adsorbed Fe^{2+} into adsorbed Fe^{3+} (Williams and Scherer, 2004; Larese-Casanova and Scherer, 2007). To better understand the adsorption behavior of a trivalent cation, we will analyze first the adsorption behavior of Al^{3+} which has been measured by Zhang et al. (1992) for the same lepidocrocite material that has been used for the adsorption study of Fe(II).

A first exploration of the modeling of the Al(III) adsorption indicated that for a good fit, the charge attribution to the 1-plane should be low (~0.1 v.u.). This low charge attribution is probably due to hydrolysis of the water ligands that are coordinated to the adsorbed Al(III). Hydrolysis is expected since Al^{3+} hydrolyzes also easily in solution. Moreover, the protons on the ligands of adsorbed Al(III) will experience a repulsive field that will stimulate the hydrolysis. We found that data are best explained if two water ligands are hydrolyzed, i.e. formation of adsorbed $Al(OH)_2^+$. Furthermore, the fitted surface charge attribution related to the adsorption option of $Al(OH)_2^+$ ($\Delta z_0 \approx 1$ v.u.) points to the formation of a bidentate complex because in that case approximately 1/3 of the Al^{3+} charge (1 v.u.) is to be found at the surface. In case of a bidentate complex, two ligands are common with the surface and the other four ligands are free (Fig. 6). The suggestion of the formation of an adsorbed $Al(III)(OH)_2^+$ complex, implies that half of the ligands in the Stern plane is hydrolyzed and the other half is not (Fig. 6). This is approximately equal to the situation that is found for the singly coordinated surface groups at the surface of for instance gibbsite. In the PPZC, half of the groups is $\equiv AlOH^{-1/2}$, while the other half is $\equiv AlOH_2^{+1/2}$. It can be shown that even in case of charging of the surface, the ratio $\equiv AlOH$:$\equiv AlOH_2$ remains relatively close to the 1:1 ratio, even at low pH, which follows from the relatively low experimental excess amount of protons in relation to the number of reactive groups. The relatively low reactivity is caused by the suppressing effect of the electrostatic field. In case of a bidentate mechanism, the adsorption reaction of Al(III) on lepidocrocite can be formulated as:

$$2{\equiv}FeOH^{-1/2} + Al^{3+}(aq) + 2H_2O(l) \Longleftrightarrow {\equiv}(FeOH)_2^{-1+\Delta z_0}Al_{III}(OH)_2^{\Delta z_1} + 2H^+(aq) \quad (10)$$

with $\Delta z_0 + \Delta z_1 = 1$ v.u.

To be more precise, we have calculated the expected CD in case of a Pauling bond valence distribution in this bidentate complex. The expected ion charge distribution is $n_0 + n_{H0} = 1 + 0 = 1$ v.u. and $n_1 + n_{H1} = 2\text{-}2 = 0$ v.u. Including the dipole effect (Eqs. (4)–(6)) with $\phi\Lambda_0 = 0$ gives $\Delta z_0 = 1.0$ v.u. and $\Delta z_1 = +0.0$ v.u. It should be noted that the same result will be found in case of the formation of a bidentate complex as result of the reaction of Al(III) with one $\equiv Fe_3O^{-1/2}$ and one $\equiv FeOH^{-1/2}$.

Using the above adsorption reaction (Eq. (10)), the final fitting was done leading to a good description of data (Fig. 6). The fitted CD parameters are $\Delta z_0 = 0.86 \pm 0.05$ v.u. and $\Delta z_1 = +0.14 \pm 0.05$ v.u. (Table 5). In case we assume the formation of bidentate complex formed from $\equiv Fe_3O^{-1/2}$ and $\equiv FeOH^{-1/2}$, the fitted CD values are $\Delta z_0 = 0.81 \pm 0.07$ v.u. and $\Delta z_1 = +0.19 \pm 0.07$ v.u. Both results point to the formation of a hydrolyzed bidentate surface complex, but the charge in the 1-plane is slightly larger than expected ($\Delta z_1 = 0$). This may be due to the formation of some additional adsorbed $AlOH^{2+}$, but its contribution could not be resolved from data.

Bidentate complex formation can be due to the formation of a double corner or a single edge surface complex. Complex formation of Al(III) on lepidocrocite has not been studied with spectroscopy. For Cd(II), the binding mode on lepidocrocite has been studied by several authors using EXAFS (Parkman et al., 1999; Randall et al., 1999; Manceau et al., 2000). At high loading, only one type of complex was found. It has a relatively short Fe-Cd distance which is characteristic for the formation of edge-linked complexes. At a lower loading, also a double corner complex is found (Manceau et al., 2000). For Cd^{2+}, formation of double edge complexes (tridentate surface complexation) has been suggested for the 001 face (Manceau et al., 2000). At the 001 and 100 faces, double corner complex formation (bidentate surface complexes) is also possible for cations. The formation of double corner complexes (bidentate surface complexes) has been reported for oxyanions, like As(III)$(OH)_3$ (Ona-Nguema et al., 2005) and As(V)O_4 (Randall et al., 2001) on lepidocrocite.

3.3.4. Fe(II) adsorption to γ-FeOOH

The adsorption behavior of Fe(II) on lepidocrocite (Fig. 7) has also been characterized with proton titrations (Zhang et al., 1992). As mentioned above, the Fe(II) adsorption can be affected by electron transfer. Such an electron transfer will lead to a significant change of the expected CD value. To assess the CD values that can be accepted as possibly due to electron transfer, we have calculated the expected Δz_0 and Δz_1 values in case of adsorption with and without electron transfer. The results are summarized in Table 6 and the details of the calculations are explained in the footnotes. Bidentate and tridentate complexes with and without electron transfer have been chosen. In case of the formation a Fe(III) surface complex, hydrolysis will occur. As argued above for Al(III), the formation of adsorbed Fe(III)$(OH)_2$ is most likely.

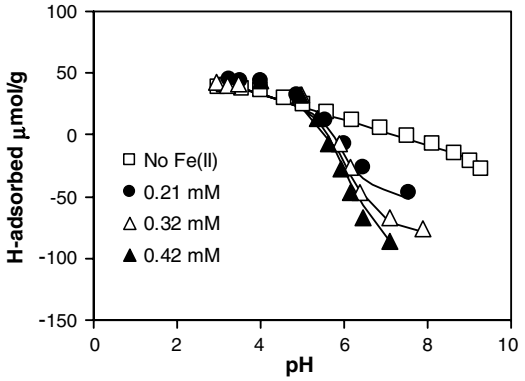

Fig. 7. The variation in the proton adsorption of lepidocrocite (10 g/l, 17.1 m^2/g) in the absence and presence of Fe(II) as function of the pH ($I = 0.6$ M NaCl). Data are from Zhang et al. (1992). The lines have been calculated using Eq. (11) and Table 5.

The calculations (Table 6) show that the surface charge attribution for the adsorption of Fe(II) as bidentate surface complex without electron transfer is almost equal to the value expected for tridentate complexes with electron transfer. A major difference is that in case of the presence of Fe(III) as central ion, the complex will hydrolyze, leading to a negative charge in the 1-plane ($\Delta z_1 < 0$). In case of bidentate complexes with and without electron transfer, the CD values for both electrostatic planes will differ.

In a first approach to model data, we have assumed bidentate Fe(II) binding without electron transfer (B-Fe(II)). Data can be described reasonably well in case of bidentate complex formation if we allow a free fit of the log$K$ and the CD value. However, the fitted charge distribution, $\Delta z_0 = 2.54 \pm 0.21$ v.u. and $\Delta z_1 = -0.54 \pm 0.21$ v.u., is certainly in conflict with the assumed mechanism. This changes if we assume the formation of a bidentate surface complex with electron transfer and subsequent hydrolysis (B-Fe(III)$(OH)_2$), using the reaction:

$$2{\equiv}FeOH^{-1/2} + Fe^{2+}(aq) + 2H_2O(l) \Longleftrightarrow {\equiv}(FeOH)_2^{-1+\Delta z_0}Fe_{III}(OH)_2^{\Delta z_1} + 2H^+(aq) \quad (11)$$

with $\Delta z_0 + \Delta z_1 = 0$ v.u. The fitted CD is $\Delta z_0 = 0.24 \pm 0.10$ v.u. and $\Delta z_1 = -0.24 \pm 0.10$ v.u. A similar CD is found, if the above reaction is written with one $\equiv FeOH^{-1/2}$ and one $\equiv Fe_3O^{-1/2}$ surface group, i.e. $\Delta z_0 = 0.20 \pm 0.09$ v.u. and $\Delta z_1 = -0.20 \pm 0.09$ v.u. The fitted CD values are within the uncertainty equal to the expected value for bidentate complex formation with electron transfer and subsequent hydrolysis, i.e. $\Delta z_0 = +0.17$ v.u., $\Delta z_1 = -0.17$ v.u. (Table 6). Apparently, the adsorbed Fe(II) seems to react as a Fe(III) ion. A noticeable difference that remains is the affinity. Comparing Data (Figs. 6 and 7) or the log$K$ values (Table 5) shows that the Al(III) ion is far more strongly bound than "Fe(III)".

Table 6
Calculated location of ion charge for bidentate (B) and tridentate (T) complexes with and without electron transfer having $\equiv FeOH^{-1/2}$ and/or $\equiv Fe_3O^{-1/2}$ as reference groups and a Pauling distribution of the central ion

Surface complex	Δz_0[a]	Δz_1[a]
$\equiv$B-Fe(II)[b]	$0 + 0.67 + 0 + 0.06 = +0.73$	$1.33 + 0 - 0.06 = +1.27$
$\equiv$T-Fe(II)[b]	$0 + 1.0 + 0 + 0.09 = +1.09$	$1.0 + 0 - 0.09 = +0.91$
$\equiv$B-Fe(III)$(OH)_2$[c]	$-1 + 1.0 + 0 + 0.17 = +0.17$	$2.0 - 2 - 0.17 = -0.17$
$\equiv$T-Fe(III)$(OH)_2$[c]	$-1 + 1.5 + 0 + 0.17 = +0.67$	$1.5 - 2 - 0.17 = -0.67$

[a] $\Delta z_0 = n_e + n_0 + n_{H0} - \phi\lambda_0$ and $\Delta z_1 = n_1 + n_{H1} + \phi\lambda_0$ (Eqs. (4)–(6)).
[b] Surface complexes without electron transfer, using $n_0 + n_1 = +2$ v.u.
[c] Surface complexes with electron transfer, using $n_0 + n_1 = +3$ v.u. Note $n_e + n_0 + n_1 = 2$ v.u.

In conclusion, we have seen so far that variation in Fe(II) binding on TiO_2 and γ-AlOOH can be linked to the local structure of the surface complexes. For Fe(II) binding to γ-FeOOH this is only possible if electron transfer is accepted, i.e. surface oxidation of adsorbed Fe(II) takes place at this ferric oxo-hydroxide surface resulting in a hydrolyzed Fe(III)$(OH)_2$ complex with an electron in the surface.

3.4. Goethite (α-FeOOH)

3.4.1. Reactive groups

Another Fe(III) oxo-hydroxide is goethite. In the lattice of goethite (α-FeOOH), two different types of triply coordinated oxygens exists, one non-protonated ($\equiv Fe_3$–O_I) and one protonated ($\equiv Fe_3$–$O_{II}H$) oxygen. The difference in proton affinity of both triply coordinated oxygens can be linked to a difference in the distances between the oxygen and the coordinating Fe-ions (Hiemstra et al., 1996b). The Fe–O distances are respectively of 196 and 210 pm, which results in bond valences of respectively 0.6 and 0.4 v.u. Both types of oxygens (O_I and O_{II}) are also found as surface groups ($\equiv Fe_3O_I^{-1/2}$ and $\equiv Fe_3O_{II}H^{-1/2}$) at the surface of the dominant 110 face and also the 100 face (Hiemstra et al., 1996b; Weidler et al., 1999; Gaboriaud and Ehrhardt, 2003). The site density of $\equiv Fe_3O_{II}H^{+1/2}$ is twice that of ($\equiv Fe_3O_I^{-1/2}$) (respectively $N_s = 6$ and 3 nm^{-2}). In case of a large difference in proton affinity for both types of triply coordinated surface groups, it can be shown that the overall charging behavior is equivalent with the use of a site density of only $N_s = 3$ nm^{-2} (Hiemstra et al., 1996b) for the triply coordinated surface groups.

Goethite has also surface groups with a lower Fe coordination, i.e. doubly and singly coordinated oxygens. The doubly coordinated $\equiv Fe_2OH$ groups are probably not proton reactive. Singly coordinated surface oxygens ($\equiv Fe_3O_I^{-3/2}$) are highly instable and are always transformed into $\equiv FeO_IH^{-1/2}$ in aqueous systems (Hiemstra et al., 1989a; Rustad et al., 1996b). Depending on the pH, the hydroxyl ($\equiv FeO_IH^{-1/2}$) may accept a second proton forming a charged surface water group ($\equiv FeO_IH_2^{+1/2}$. The site density is 3 nm^{-2} at the 110 face.

In the present approach, the affinity constants of both proton reactive surface groups ($\equiv FeOH^{-1/2}$ and

Table 7
Location of ion charge and affinity constants used to describe the charging behavior, the Fe(II) (Dixit and Hering, 2006) and the Al(III) (Lövgren et al., 1990) adsorption of goethite

Surface group	Δz_0	Δz_1	Δz_2	log$K$
$\equiv FeOH^{-1/2}$	0	0	0	0
$\equiv FeOH_2^{+1/2}$	1	0	0	9.2
$\equiv FeOH^{-1/2}$–Na[a]	0	1	0	−0.60
$\equiv FeOH_2^{+1/2}$–Cl[a]	1	−1	0	9.2–0.45 = 8.75
$\equiv FeOH_2^{+1/2}$–NO_3[a]	1	−1	0	9.2–0.7 = 8.5
$\equiv FeOH_2^{+1/2}$–ClO_4[b]	1	−1	0	9.2–1.4 = 7.8
$\equiv$(FeOH)$_2$–Al$(OH)_2$[c]	0.95 ± 0.03	0.05 ± 0.03	0	1.51 ± 0.08
$\equiv$(FeOH)$_2$–Fe_{II}[d]	$\equiv$0.73[e]	$\equiv$1.27	0	8.47 ± 0.05
$\equiv$(FeOH)$_2$–$Fe_{III}(OH)_2$[d]	$\equiv$0.17[e]	$\equiv$−0.17	0	−9.31 ± 0.08
$\equiv$(FeO)$_2$$As_{III}OH$[g]	$\equiv$0.34[f]	$\equiv$−0.34[f]	0	7.26 to 6.58
$\equiv FeOAs_{III}(OH)_2$[g]	$\equiv$0.16[f]	$\equiv$−0.16[f]	0	4.91 to 4.62
$\equiv FeOAs_{III}(OH)_3Fe_{II}$[h]	0.08 ± 0.05	+0.92 ± 0.05	0	3.38 ± 0.10

[a] log$K$ from Rahnemaie et al. (2007).
[b] log$K$ fitted on data of Rietra et al. (2000a).
[c] Defined in Eq. (14).
[d] Defined in Eqs. (16) and (17) as Fe^{2+} adsorption without and with electron transfer.
[e] Taken by definition from Table 6.
[f] Taken from Stachowicz et al. (2006).
[g] log$K$ values vary for the bidentate complex between the various goethite preparations. See text. Reactions defined in Eqs. (18) and (19).
[h] Defined in Eq. (20).

$\equiv Fe_3O_{II}{}^{-1/2}$) are set equal in the modeling (Hiemstra and van Riemsdijk, 1996a,b).

Faces like the 021 and 001 face terminate the goethite needles at the top ends of the crystals (Spadini et al., 2003). These crystal faces have equal numbers of singly and doubly coordinated surface groups ($N_s = 7$–$8\ nm^{-2}$). In the modeling, the protonation constant of these singly coordinated surface groups is taken equal to that of the 110 face. The overall site density of the singly coordinated surface groups of goethite is calculated assuming 90% 110/100 face and 10 % 021/001 face, leading to $2.7 + 0.75 = 3.45\ nm^{-2}$ for the singly coordinated group (Hiemstra and van Riemsdijk, 1996a). The overall net site density of the reactive triply coordinated surface group is $2.7\ nm^{-2}$.

3.4.2. Surface charge

Based on the above analysis, the surface charging can be calculated using two protonation reactions:

$$\equiv FeO_IH^{-1/2} + H^+(aq) \Longleftrightarrow \equiv FeO_IH_2^{-1/2+\Delta z_0} \quad (12)$$

and

$$\equiv Fe_3O_{II}^{-1/2} + H^+(aq) \Longleftrightarrow \equiv Fe_3O_{II}H^{-1/2+\Delta z_0} \quad (13)$$

In the Fe(II) adsorption modeling, we have used the proton affinity constant of $\log K_H = 9.2$ for both groups (Hiemstra and van Riemsdijk, 1996a). The ion pair formation constants, given in Table 7, are from Rahnemaie et al. (2007). In the modeling, a capacitance value of 0.93 F/m^2 (well-structured goethite) is used.

3.4.3. Al^{3+} adsorption on goethite

Before analyzing the behavior for Fe(II), we will first focus on the Al(III) adsorption, similar as we have done for lepidocrocite. Data are from Lövgren et al. (1990), who titrated goethite in the presence of different initial concentrations of Al(III) in 0.1 M $NaNO_3$ (Fig. 8). As will be discussed below, the charge distribution is most closely explained by the formation of a bidentate complex. Similar as for lepidocrocite, we also find in this case a strong hydrolysis, i.e. binding as $Al(OH)_2{}^+$. The proposed complex can be formed at the 110 face, most likely as a double corner complex. The reaction can be formulated as:

$$2{\equiv}FeOH^{-1/2} + Al^{3+}(aq) + 2H_2O(l) \Longleftrightarrow \equiv(FeOH)_2^{-1+\Delta z_0}Al_{III}(OH)_2^{+\Delta z_1} + 2H^+(aq) \quad (14)$$

with $\Delta z_0 + \Delta z_1 = 1$ v.u. As for lepidocrocite, the expected overall charge distribution for the formation of this complex is $\Delta z_0 = 1.0$ v.u. and $\Delta z_1 = +0.0$ v.u. if a Pauling bond valence attribution is valid. We have calculated the geometry of this surface complex using MO/DFT computations applying various DFT models. The calculation approach is described in Hiemstra and van Riemsdijk (2006). The bond lengths of the Al with the surface groups are given in Table 8. The bond lengths vary with the type of ligands involved (common OH, free OH and OH_2). Application of the Brown's bond valence principle results in $n_0 + n_{H0} = 1.03 \pm 0.05$ v.u. and $n_1 + n_{H1} = -0.03 \pm 0.05$ v.u. The uncertainty (± 0.05) is estimated based on our previous experience that the precise value depends on the model used, the hydration and the defined FeOOH cluster (Hiemstra and van Riemsdijk, 2006; Stachowicz et al., 2006; Hiemstra et al., 2007; Rahnemaie et al., 2007). The dipole correction term is negligible, leading to a set of CD coefficients of $\Delta z_0 = 1.03$ v.u. and $\Delta z_1 = -0.03$ v.u. Although the individual bond length and valences are quite different, the calculated CD is almost equal to the Pauling estimate within the uncertainty.

In the modeling, the primary proton adsorption data were fitted first. It results in $\log K_H = 9.09 \pm 0.07$ and the capacitance $C_1{\equiv}C_2 = 1.06 \pm 0.02\ F/m^2$ for data of Fig. 8. Next, the titration data with added Al(III) were fitted resulting in a set of charge distribution values

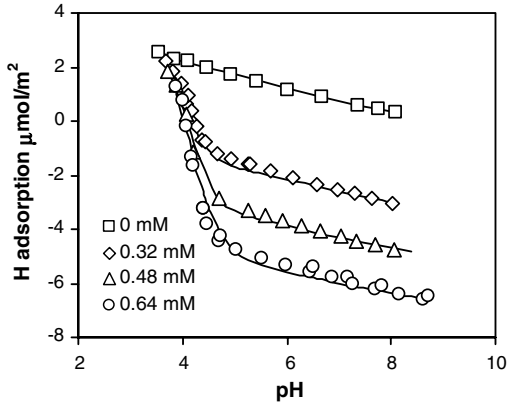

Fig. 8. The variation in the proton adsorption of goethite (7.16 g/l, 39.9 m^2/g) in the absence and presence of Al(III) as function of the pH ($I = 0.1$ M $NaNO_3$). Data are from Lövgren et al. (1990). The lines have been calculated using Eq. (14) and Table 7. The capacitance and $\log K_H$ have been adjusted to the values given in the text.

Table 8
The calculated distances (pm) in the geometry of bidentate $Al(OH)_2$ complex using various DFT models

Bond	B3LYP	EDF1	EDF2	Exp
FeOH–Al	192.4	193.1	191.3	
FeOH–Al	192.6	192.9	191.2	—
Al-OH	180.8	182.3	183.9	—
Al-OH	183.7	182.5	180.5	—
Al-OH_2	204.7	208.1	202.6	—
Al-OH_2	219.7	225.6	216.4	
FeOH	195.5 ± 0.2	198.3 ± 0.3	193.8 ± 0.2	196[a]
Fe–Al	360 ± 1	363 ± 1	356 ± 1	355 ± 3[b]
R_0	167.8	169.0	166.9	165.1[c]
n_0[d]	+1.03	+1.05	+1.03	
n_1[d]	−0.03	−0.05	−0.03	

[a] Distance present in the goethite structure without relaxation.
[b] The Fe–Ga distance characteristic for double corner complexation is d(Fe–Ga) = 355 ± 3 pm (Persson et al., 2006).
[c] Average R_0 for Al in minerals.
[d] The charge of $Al(OH)_2^+$ attributed to the ligands of the 0- and 1-plane application of the Brown bond valence concept to the calculated geometry, using $s = \exp((R_0 - R)/37)$ in which s is the bond valence, R the bond length and R_0 the Al specific constant.

$\Delta z_0 = +0.95 \pm 0.03$ v.u. and $\Delta z_1 = +0.05 \pm 0.03$ v.u.. The CD value agrees with the above calculated value within the range of uncertainties, i.e. the dominant binding mechanism is probably a bidentate complex with the hydrolysis of two outer ligands. We note that the formation of bidentate complexes on goethite has frequently been reported in EXAFS studies for metal ions like for Cd(II) (Manceau et al., 2000), Cu(II) (Peacock and Sherman, 2004), Zn(II) (Waychunas et al., 2002) and Hg(II) (Kim et al., 2004).

3.4.4. Fe(II) on goethite

The Fe(II) adsorption of goethite has recently been measured extensively by (Dixit and Hering, 2006). The binding of Fe(II) was found to be reversible. Data are given in Fig. 9. The modeling of data has been done in several steps. A primary modeling indicates that in case of binding as Fe(II) ion without electron transfer, the charge attribution is relatively high, i.e. $\Delta z_0 \approx 1.2$ v.u.. Such a value is more representative for the formation of a tridentate surface complex than for the formation of a bidentate surface complex. Tridentate surface complexes can be formed at the 021 face, as has been found for Cd(II) (Spadini et al., 1994; Manceau et al., 2000), but the total Fe(II) loading in the experiments of (Dixit and Hering, 2006) is relatively high which implies that the 110 face has to accommodate a considerable part of the ferrous ions. In principle, tridentate complexes can be formed at the 110 face at interaction with two $\equiv$FeOH and one $\equiv Fe_3O$ (double edge sharing), according to,

$$2{\equiv}\mathrm{FeOH}^{-1/2} + 1(\mathrm{l}) \equiv \mathrm{Fe_3O}^{-1/2} + \mathrm{Fe}^{2+}(\mathrm{aq}) \Longleftrightarrow \equiv(\mathrm{FeOH})_2(\mathrm{Fe_3O})^{-1.5+\Delta z_0}\mathrm{Fe}_{\mathrm{II}}^{\Delta z_1} \quad (15)$$

with $\Delta z_0 + \Delta z_1 = 2$. Using this reaction, the CD values, obtained in a very good fit ($R^2 = 0.986$), are $\Delta z_0 = 1.26 \pm 0.03$ v.u. and $\Delta z_1 = 0.74 \pm 0.03$ v.u. The fitted Δz_0 value is larger than the expected value of $\Delta z_0 = 1.09$ (Table 6), but the formation of a tridentate complex cannot be excluded definitively. However, as noted above, divalent ions usually form double corner bidentate surface complexes at the 110 face. Tridentate complex formation has only been suggested for the Pb(II)ion (Bargar et al., 1997b). The Pb(II) ion is probably exceptionable since this ion is able to change its coordination and bond valence drastically upon adsorption (CN = 3). From this perspective, one may consider bidentate complex formation for Fe(II) at the 110 face as more likely. If this is the case, the Fe(II) adsorption is maybe a combination of an adsorption process with and without electron transfer. Unfortunately, the fitting procedure is unable to generate for this data a set of reliable CD and log$K$ values if two reactions are assumed to occur simultaneously (4-parameter fit). To reduce the number of parameters, we have fixed the CD values to calculated values for bidentate (B) and tridentate (T) complexation as given in Table 6. Several options were explored. In case of bidentate complexation, the fit for the combination B-Fe(II) and B-Fe(III)$(OH)_2$ surface complex gives the best result ($R^2 = 0.980$): The reactions are:

$$2{\equiv}\mathrm{FeOH}^{-1/2} + \mathrm{Fe}^{2+}(\mathrm{aq}) \Longleftrightarrow \equiv(\mathrm{FeOH})_2^{-1+\Delta z_0}\mathrm{Fe}_{\mathrm{II}}^{\Delta z_1} \quad (16)$$

with $\Delta z_0 + \Delta z_1 = 2$ and

$$2{\equiv}\mathrm{FeOH}^{-1/2} + \mathrm{Fe}^{2+}(\mathrm{aq}) + 2\mathrm{H_2O(l)} \Longleftrightarrow \equiv(\mathrm{FeOH})_2^{-1+\Delta z_0}\mathrm{Fe_{III}(OH)}_2^{\Delta z_1} + 2\mathrm{H}^{+}(\mathrm{aq}) \quad (17)$$

with $\Delta z_0 + \Delta z_1 = 0$. The fitted log$K$values have been given in Table 7. The model lines are in Fig. 9. We note that other combinations like B-Fe(II) & T-Fe(III)$(OH)_2$ cannot be excluded on the basis of the quality of the fit ($R^2 = 0.978$). It shows that the model is flexible enough to describe data, i.e.

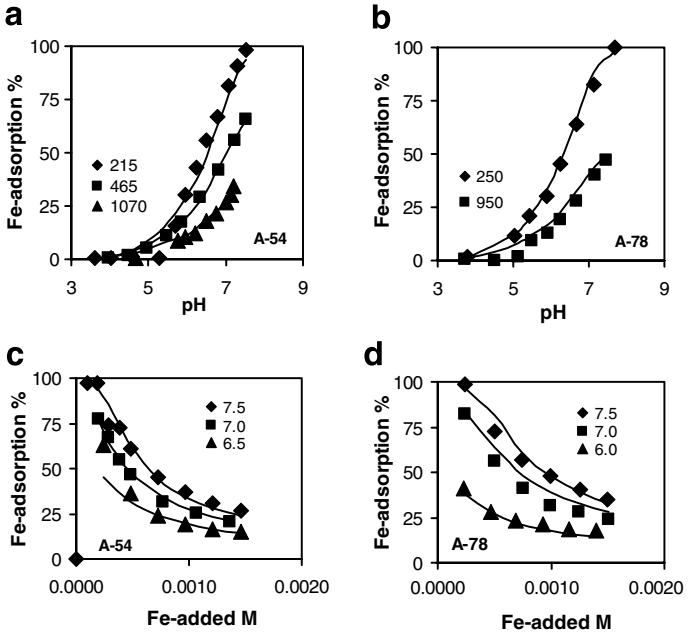

Fig. 9. Adsorption edges of Fe(II) on two goethites (2.5 g/l) as function of pH and loading in 0.01 M NaCl. (a and b) Surface area = 54 m^2/g and (c and d) Surface area = 78 m^2/g. Data are from Dixit and Hering (2006). The lines are calculated with the parameters of Table 7.

in this case the precise mechanism can only be proposed based on additional considerations.

To understand the conditions that favor electron transfer, we have calculated the relative contribution of adsorbed Fe^{2+} and adsorbed "$Fe(III)(OH)_2$" as function of pH and loading (Fig. 10). The adsorption of $Fe(OH)_2$ is more pH dependent than the adsorption of Fe(II) species. It implies that the surface oxidation becomes relatively more important at high pH. At pH $< \sim$7, adsorbed ferrous iron is present as adsorbed Fe^{2+} while above pH $> \sim$7.5, it is adsorbed as a $Fe(III)(OH)_2$ ion with electron transfer to the solid. This agrees with a recent Mössbauer study, showing that the ratio of Fe(II)/Fe(III) adsorbed to montmorillonite is reversible and decreases at high pH (Gehin et al., 2007).

3.4.5. *Fe(II)–As(III) interaction*

Dixit and Hering (2006) have also measured the influence of As(III) on the Fe(II) adsorption and *vice versa* for one of their goethite preparations (A78). To predict the effect of the presence of As(IIII) on the adsorption Fe(II) on goethite, first the adsorption behavior of As(III) will be parameterized.

The main surface species of As(III) on goethite is a bidentate complex (Ona-Nguema et al., 2005). It is formed by interaction of $As(III)(OH)_3$ with singly coordinated surface groups on the main crystal face of goethite (Sun and Doner, 1996). In addition, a monodentate complex may be present in a minor amount. This species contributes at high loading (Stachowicz et al., 2006). The reactions can be formulated as:

$$2{\equiv}FeOH^{-1/2} + As(OH)_3^0(aq) \Longleftrightarrow {\equiv}(FeO)_2^{-1+\Delta z_0}As(OH)^{\Delta z_1} + 2H_2O(l) \quad (18)$$

and

$$1{\equiv}FeOH^{-1/2} + As(OH)_3^0(aq) \Longleftrightarrow {\equiv}FeO^{-1/2+\Delta z_0}As(OH)_2^{\Delta z_1} + 1H_2O(l) \quad (19)$$

with $\Delta z_0 + \Delta z_1 = 0$.

Dixit and Hering (2003) have measured the As(III) adsorption for one of the goethites (A54) extensively. Unfortunately, for the goethite on which Fe(II)–As(III) interaction has been measured (A78) only a few data points are available at zero addition of Fe(II) (Fig. 11b). To model data, we used the CD values for As(III) surface complexes that have been calculated by Stachowicz et al. (2006). These charge distribution coefficients (Table 7) have been derived from the geometries of the As(III) surface complexes, found by molecular orbital (MO) optimization using Density Functional Theory (DFT). Data for A54 could be described well with $\log K({\equiv}(FeO)_2AsOH) = 6.86 \pm 0.04$ and $\log K({\equiv}FeOAs(OH)_2) = 4.86 \pm 0.05$ ($R^2 = 0.987$). Application to the sparingly available data for the A78 goethite systems without added Fe(II) leads to a too high prediction of the As(III) adsorption. We have further adapted the log$K$ values by fitting the log$K$ values for the small data set of A78, leading to respectively $\log K({\equiv}(FeO)_2AsOH) = 6.56 \pm 0.47$ and $\log K({\equiv}FeOAs(OH)_2) = 4.62 \pm 0.13$, which have been used in the final fitting of the Fe(II) adsorption.

Application of these parameters to the Fe(II)–As(II) system leads to the prediction of a strong reduction of the As(III) adsorption (dotted line in Fig. 11b). The main reason is site competition, which is most prevalent at high pH, where both ions have the highest adsorption in the monosorbate systems. The amounts of As(III) and Fe(II) added in the dual-sorbate systems are both high, equivalent with

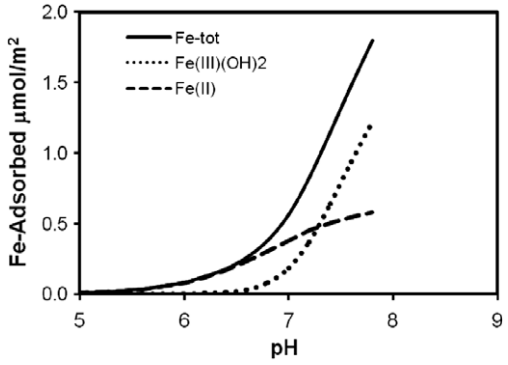

Fig. 10. The total Fe(II) adsorption (full line) on goethite as function of pH, made up by a contribution of the Fe(II) species (dashed line) and $Fe(OH)_2$ species (dotted line) as function of pH in 0.01 M NaCl at an equilibrium concentration of 0.5 mM Fe(II).

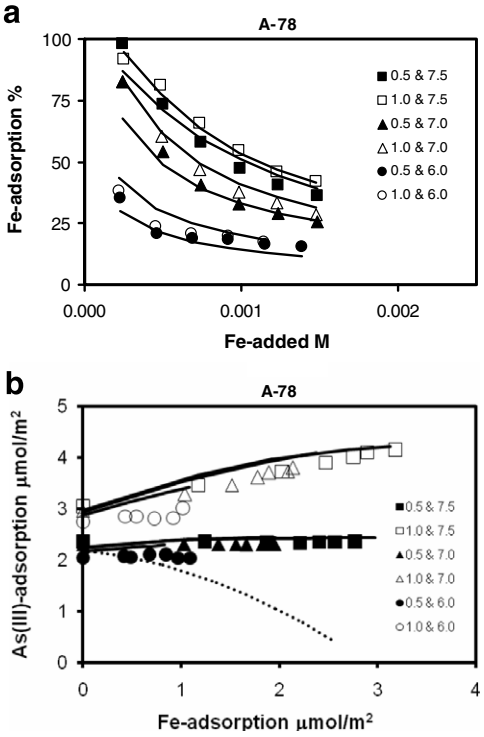

Fig. 11. (a) Adsorption edges of Fe(II) for As(III)–Fe(II) goethite systems (2.5 g/l) in 0.01 M NaCl for pH = 6, 7 and 7.5 and an initial As(III) concentration of 0.5 or 1 mM As. (b) The adsorption of As(III) as function of the adsorption of Fe(II), corresponding to the data of (a). Data are from Dixit and Hering (2006). The full lines are calculated with the parameters of Table 7. The dotted line refers to the As(III) adsorption at pH 6 without formation of the ternary Fe(II)–As(III) surface complex.

a loading of 2–3 μmol/m^2 for each element. It implies that the large majority of singly coordinated surface groups is used to accommodate all these ions. The experimental data show even an increase of As(III) loading with increase of the Fe(II) loading. The strong increase may point to the formation of a ternary complex or for instance surface precipitation. Modeling shows that any ternary complex has to be a monodentate surface complex, due to the lack of free sites at the surface. Data could be described well assuming that the monodentate As(III) surface complex (Eq. (19)) may interact with a Fe(II) ion. The relevant formation reaction that can describe data well can be formulated as:

$$\equiv FeOH^{-1/2} + As(OH)_3^0(aq) + Fe^{2+}(aq) \Longleftrightarrow \equiv FeO^{-1/2+\Delta z_0}As(OH)_2Fe_{II}OH^{\Delta z_1} + H^+(aq) \quad (20)$$

with $\Delta z_0 + \Delta z_1 = +1$. Our modeling suggests the release of one proton at the formation of a Fe(II)–As(III) surface complex (Eq. (20)). Proton release may for instance be due to the formation of an OH ligand in the Fe(II) coordination sphere or the change in the coordination number of the As(III) from CN = 3–4 for $As(OH)_3{}^0$ to $As(OH)_4{}^{-1}$ or the formation of an As–O–Fe bond. These details are difficult to resolve here. We have fitted the CD value and the log$K$ on the Fe(II) adsorption data (Fig. 11a) and tested the results by looking to the predicted corresponding As(III) binding (Fig. 11b). The fit on the Fe(II) data leads to $\Delta z_0 = 0.08 \pm 0.05$ $\Delta z_1 = 0.92 \pm 0.05$ v.u. and $\log K = 3.50 \pm 0.12$. The fitted CD value is in agreement with what is expected for the formation of a As(III) monodentate surface complex. The CD of a hydrated monodentate $\equiv FeOAs(OH)_2$ complex is $\Delta z_0 = 0.09$ and $\Delta z_1 = -0.09$ v.u. (Stachowicz et al., 2006), when calculated with the MO/DFT geometry approach (Hiemstra and van Riemsdijk, 2006). It is interesting to note the $\equiv FeO–As(OH)_2Fe_{II}OH$ can be considered as a binuclear-bidentate complex. At the surface of goethite, binuclear-bidentate surface complexes are found to be dominant (Ona-Nguema et al., 2005). The fitted Fe(II) adsorption is given in Fig. 11a as lines. The corresponding prediction of the As(III) binding is given in Fig. 11b.

3.5. HFO

The experimental information with respect to the Fe(II) binding by (2-line) ferrihydrite is very sparse (Liger et al., 1999; Appelo et al., 2002). In the reported experiments, sulphate is present since Fe(II) has been added as Fe(II)SO_4. Moreover, the Fe(II) binding has been measured in $NaNO_3$ and both data sets are, according to Appelo et al., not fully consistent. For these reasons, our modeling will be a first-order approach.

The structure of 2-line ferrihydrite or hydrous ferric oxide (HFO) has been discussed recently by (Spadini et al., 2005). The structure of HFO and goethite is related. Two characteristic Fe–O bond lengths are found (Combes et al., 1989; Waychunas et al., 1993), i.e. d-FeO $\approx$ 195 ± 1 pm and d-FeOH = 209 ± 1 pm, which are close to the two Fe–O distances found in goethite. The fundamental unit of a synthetic 2-line ferrihydrite is the $Fe(O,OH)_6$ octahedron present in double chains which are cross-linked. The inter-chain linkage is probably disordered which may result in smaller Fe–Fe distances (Waychunas et al., 1993). Similar as for goethite, the structure of HFO gives rise to the presence of singly, doubly, and triply coordinated surface groups. The relative short chain length of the crystals will enhance the number of singly coordinated surface groups at the expense of triply coordinated surface groups. In case of an equal fraction of "1 1 0- and 0 2 1-like" faces, three-quarters of the apparent reactive surface sites might be singly coordinated surface groups. In the modeling, the site density of both groups is set at respectively N_s ($\equiv FeOH$) = 6 nm^{-2} and N_s ($\equiv Fe_3O$) = 2 nm^{-2}. In addition, the site density of the doubly coordinated group is arbitrarily set equal to the density of the singly coordinated groups N_s ($\equiv Fe_2OH$) = 6 nm^{-2}. For modeling the particle charge, we have used the capacitance values and the ion pair formation constants as found for goethite (Table 7) and the proton affinity constants of the proton reactive surface groups are set equal to the PZC (PZC = 8.2). An effective surface area A_{eff} of 600 m^2/g has been used (Davis and Leckie, 1978b). As discussed later, this number may be doubted in Fe(II)-HFO systems.

The adsorption behavior is probably dominated by the crystal faces that terminate the chains (0 2 1/0 0 1 like faces). At the 0 2 1 face, ions may form tridentate complexes, as shown for Cd(II) (Spadini et al., 2003). The Cd^{2+} ion interacts with 1 doubly and two singly coordinated surface groups. If Fe(II) adsorbs at the same position, the reaction is:

$$2\equiv FeOH^{-1/2} + 1\equiv Fe_2OH^0 + Fe^{2+}(aq) \Longleftrightarrow \equiv(FeOH)_2(Fe_2OH)^{-1+\Delta z_0}Fe(II)^{\Delta z_1} \quad (21)$$

with $\Delta z_0 + \Delta z_1 = 2$. In case of a Pauling distribution, we have an equal ion charge distribution over both electrostatic planes. The calculated overall CD values are $\Delta z_0 = 1.0$ v.u. and $\Delta z_1 = 1.0$ v.u.

In the modeling, we have applied the above reaction and fitted the CD values of $\Delta z_0 = 1.30 \pm 0.16$ v.u. and $\Delta z_1 = 0.70 \pm 0.16$ v.u. The value of Δz_0 is too high compared to the above expected value which may indicate that also surface oxidation may occur via electron transfer to the solid and a subsequent hydrolysis of the ligands. This is supported by recent Mössbauer spectroscopy (Silvester et al., 2005). The reaction can be formulated as:

$$2\equiv FeOH^{-1/2} + 1\equiv Fe_2OH^0 + Fe^{2+}(aq) + 2H_2O(l) \Longleftrightarrow \equiv(FeOH)_2(Fe_2OH)^{-1+\Delta z_0}Fe_{III}(OH)_2^{\Delta z_1} + 2H^+(aq) \quad (22)$$

with $\Delta z_0 + \Delta z_1 = 0$. The CD coefficients for this tridentate reaction are expected to be $\Delta z_0 = +0.59$ v.u. and $\Delta z_1 = -0.59$ v.u. Following the same approach as done for goethite, i.e. fixing the CD values to the above expected values, we have fitted the adsorption edge using both reactions resulting in a good fit with $\log K(Fe_{II}) = 4.59 \pm 0.12$ and $\log K(Fe_{III}(OH)_2) = -13.07 \pm 0.38$ ($R^2 = 0.98$) as shown in Fig. 12a.

More recently, Appelo et al. (2002), have measured the Fe(II) adsorption using the same experimental approach as (Liger et al., 1999), but using a higher solid:solution ratio. The result, a measured adsorption isotherm at pH ~7,

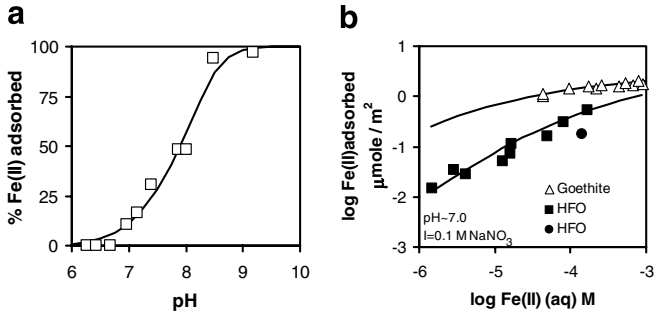

Fig. 12. (a) Adsorption edge of Fe(II) (0.16 mM) on 2-line ferrihydrite, HFO (0.21 g/l) as function of pH in 0.1 M $NaNO_3$. Data are from Liger et al. (1999). (b) Adsorption isotherms of Fe(II) for goethite (open symbols) and HFO (closed symbols) at pH ~7 in 0.1 M $NaNO_3$. For HFO, the black squares are from Appelo et al. (2002) and the black sphere is from Liger et al. (1999). The lines have been calculated. See text in Sections 3.5 and 3.6.

is given in Fig. 12b with black squares. For comparison, also the Fe(II) adsorption found by Liger et al. is given (black sphere), showing that both data sets are not completely consistent. The adsorption isotherm can be described well if the above log$K$ values, fitted to the adsorption edge of Fig. 12a, are both increased by about 0.8 log$K$ units, resulting in the lower line in Fig. 12b through the HFO data points.

3.6. General discussion

The Fe(II) interaction with non-ferric minerals differs from ferric-minerals. In the modeling of the Fe(III) minerals, we have found indications of interfacial electron transfer upon Fe^{2+} adsorption, that may change the overall CD value. For lepidocrocite, the surface oxidation is apparently complete, whereas for goethite and HFO, two types of surface species might be present. The formation reaction for both types of surface species can be combined and written as a chemical equilibrium between $\equiv S_{III}$–Fe_{II} and $\equiv S_{II}$–$Fe_{III}(OH)_2$. The resulting internal redox reaction reads:

$$\equiv S_{III} - Fe_{II} + 2H_2O \Longleftrightarrow \equiv S_{II} - Fe_{III}(OH)_2 + 2H^+ \qquad (23)$$

The log$K$ value follows from the difference in log$K$ values of the formation reactions of both surface species. For goethite, we find $\Delta \log K = -9.31 + -8.47 \approx -17.8 \pm 0.1$. For HFO, $\Delta \log K == -13.07 + -4.59 \approx -17.7 \pm 0.5$. The calculation shows that, despite large differences in the constituting log$K$ values for both minerals, the log$K$ for the equilibrium between adsorbed Fe(II), with and without electron transfer (Eq. (23)), is equal within the uncertainties.

The intrinsic log$K$ value of Eq. (23) can be interpreted as a combination of an electron transfer reaction (logK_E) and a deprotonation of two OH_2 ligands ($-\log K_H$), producing $\equiv Fe(III)(OH)_2$. The latter one is contributing most to the standard Gibbs free energy change of the reaction given. If the protonation constant of a Fe(III)-OH ligand is about $\log K_H = 8 \pm 1$, the intrinsic logK_E value for the electron transfer will be $\log K_E \leqslant \approx 2 \pm 2$. It is important to note that the log$K$ found for the above redox reaction (Eq. (23)) cannot be applied to lepidocrocite. The formation of S(II)–$Fe(III)(OH)_2$ is relatively stronger, which might point to a higher electron transfer affinity (logK_E) for this mineral. At present, an explanation is speculative. Maybe, it is related to the difference in mineral structure (Manceau et al., 2000). We note that very recently no Fe^{2+} species could be detected for hematite with Mössbauer spectroscopy in the normal concentration range (Larese-Casanova and Scherer, 2007), suggesting that also for this mineral all adsorbed Fe(II) has been transformed by electron transfer.

The location of the electron in the mineral is also unknown, i.e. "Is it at the surface as part of a defined complex, or is it present at certain defects in the mineral bulk?" This cannot be resolved with current electrostatic double layer models because the location of the charge within the lattice is conceptually not relevant for the electrostatic field radiating from the surface. In the case that the electrons move to defects, a mineral with a low surface area and a high defect density is favored in the surface oxidation reaction.

For goethite, reversibility of the adsorption has been claimed (Dixit and Hering, 2006). In other cases, adsorbed Fe(II) could not be extracted and this was attributed to instability of the lattice leading to transformation to a Fe(III)/Fe(II) mineral (Jeon et al., 2003). If both processes occur simultaneously, the final outcome will be time, pH and material dependent.

Our speciation calculation (Fig. 10) has shown that the above reaction is favored by a high pH value. For HFO, we calculate that at pH = 7 (Fig. 12b), the adsorption isotherm is fully dominated by the adsorption of Fe(II), i.e. no surface oxidation yet. This is also found for goethite. A noticeable difference between goethite and HFO is the apparently much higher affinity of the Fe^{2+} ions for goethite than for HFO, as is illustrated in Fig. 12b with the experimental (triangles) and calculated adsorption isotherm of Fe(II) on goethite (upper line). The reason is unknown. A possible explanation might be an incorrect use of a high surface area for HFO. According to Hansel et al. (2005) and Pedersen et al. (2005), the presence of Fe^{2+} strongly catalyzes the transformation of HFO to other minerals like goethite and lepidocrocite. The transformation may be already significant at the time scale of the adsorption experiments (hours). It might imply that the surface area used is too high leading to a too low experimental loading if expressed per unit surface area.

Above pH ~7.5, surface oxidation with electron transfer to the solid is expected to dominate. The overall reaction is

driven by the deprotonation of the $-OH_2$ ligands, as also follows from the mass action law of Eq. (23), i.e. the release of two protons. In contrast, one expects that the electron transfer itself will be favored by a low pH, because of the positive surface charge for these conditions. The positive surface potential attracts the electron that can be released by the adsorbed Fe(II), leading to interfacial redistribution of charge.

4. CONCLUSIONS

- At the surface of non-ferric (hydr)oxides, divalent iron is bound without electron transfer. At ferric (hydr)oxides, adsorbed Fe(II) may transfer an electron to the solid, creating a trivalent ion that will hydrolyze. The complex formed is equivalent with adsorbed $Fe(OH)_2$.
- The charge distribution of Fe(II), adsorbed on the surface of TiO_2 without hydrolysis, is characteristic for the formation of a quattro-dentate surface complex. Such complexes have recently been found for a series of mono-, di- and trivalent cations with spectroscopy.
- The charge distribution of Fe(II), adsorbed on the surface of γ-AlOOH (boehmite), points to the formation of a tridentate surface complex. Such type of surface complexes have also been found for Ni(II) using EXAFS.
- The titration data of Fe(II)–lepidocrocite can be explained as due to a complete surface oxidation of adsorbed divalent iron via electron transfer to the solid. The experimental Fe(II) adsorption data of goethite and HFO can be explained by Fe(II) binding with and without electron transfer.
- Goethite and HFO react quite similar with respect to electron exchange between an adsorbed ferrous ion and a ferric ion of the mineral lattice. However, the affinity of Fe(II) for goethite is significantly larger than for HFO.
- Surface oxidation is favored by a high pH value, since it is dominantly driven by the deprotonation of Fe_{III}-OH_2 ligands. Surface oxidation dominates above pH ~7.5, while Fe(II) is present below pH ~7 as an adsorbed Fe^{2+} ion.
- At the goethite surface, Fe(II) and As(III) may form a ternary surface complex in which As(III) is present as a binuclear bidentate complex.

ACKNOWLEDGMENTS

Part of this work was funded by the TRIAS project 835.80.006/Delft Cluster 5.17, and by the EU project, FUNMIG (516514, F16W-2004). We thank Dr M. K. Ridley for sharing information for the charging behavior of rutile. In addition, we thank three anonymous reviewers and the associated editor for their comments.

REFERENCES

Amonette J. E., Workman D. J., Kennedy D. W., Fruchter J. S. and Gorby Y. A. (2000) Dechlorination of carbon tetrachloride by Fe(II) associated with goethite. *Environ. Sci. Technol.* **34**(21), 4606–4613.

Appelo C. A. J., van der Weiden M. J. J., Tournassat C. and Charlet L. (2002) Surface complexation of ferrous iron and carbonate on ferrihydrite and the mobilization of arsenic. *Environ. Sci. Technol.* **36**(14), 3096–3103.

Ballesteros M. C., Rueda E. H. and Blesa M. A. (1998) The influence of iron (II) and (III) on the kinetics of goethite dissolution by EDTA. *J. Colloid Interf. Sci.* **201**(1), 13–19.

Bargar J. R., Brown, Jr., G. E. and Parks G. A. (1997b) Surface complexation of Pb(II) at oxide–water interfaces: II. XAFS and bond-valence determination of mononuclear pb(II) sorption products and surface functional groups on iron oxides. *Geochim. Cosmochim. Acta* **61**, 2639–2652.

Boily J. F., Lützenkirchen J., Balmès O., Beattie J. and Sjöberg S. (2001) Modeling proton binding at the goethite (α-FeOOH)-water interface. *Colloids Surf. A* **179**(1), 11–27.

Bokhimi X., Sanchez-Valente J. and Pedraza F. (2002) Crystallization of sol–gel boehmite via hydrothermal annealing. *J. Solid State Chem.* **166**(1), 182–190.

Bokhimi X., Toledo-Antonio J. A., Guzman-Castillo M. L. and Hernandez-Beltran F. (2001) Relationship between crystallite size and bond lengths in boehmite. *J. Solid State Chem.* **159**(1), 32–40.

Bonneville S., Behrends T., van Cappellen P., Hyacinthe C. and Roling W. F. M. (2006) Reduction of Fe(III) colloids by shewanella putrefaciens: a kinetic model. *Geochim. Cosmochim. Acta* **70**(23), 5842–5854.

Bourikas K., Hiemstra T. and van Riemsdijk W. H. (2001) Ion pair formation and primary charging behaviour of titanium oxide (anatase and rutile). *Langmuir* **17**(3), 749–756.

Brown I. D. (2002) *The chemical bond in inorganic chemistry: the bond valence model*. Oxford University Press, Oxford.

Brown I. D. and Altermatt D. (1985) Bond-valence parameters obtained from a systematic analysis of the inorganic crystal structure database. *Acta Cryst.* **B41**, 244–247.

Buerge I. J. and Hug S. J. (1999) Influence of mineral surfaces on Chromium(VI) reduction by Iron(II). *Environ. Sci. Technol.* **33**(23), 4285–4291.

Catalano J. G., Park C., Zhang Z. and Fenter P. (2006) Termination and water adsorption at the alpha-Al_2O_3 (012)—aqueous solution interface. *Langmuir* **22**(10), 4668–4673.

Charlet L., Bosbach D. and Peretyashko T. (2002) Natural attenuation of TCE, As, Hg linked to the heterogeneous oxidation of Fe(II): an AFM study. *Chem. Geol.* **190**(1–4), 303–319.

Choi S., Hong S., Ahn K. and Baumann E. R. (2001) Adsorption of ferrous iron on the lepidocrocite surface. *Environ. Technol.* **22**(3), 355–365.

Combes J. M., Manceau A., Calas G. and Bottero J. Y. (1989) Formation of ferric oxides from aqueous-solutions—a polyhedral approach by X-ray absorption-spectroscopy .1. hydrolysis and formation of ferric gels. *Geochim. Cosmochim. Acta* **53**(3), 583–594.

Connor P. A., Dobson K. D. and McQuillan A. J. (1999a) Infrared spectroscopy of the TiO_2/aqueous solution interface. *Langmuir* **15**, 2402–2408.

Davies S. H. R. and Morgan J. J. (1989) Manganese(II) oxidation-kinetics on metal–oxide surfaces. *J. Colloid Interf. Sci.* **129**(1), 63–77.

Davis J. A., James R. and Leckie J. O. (1978a) Surface ionization and complexation at the oxide/water interface. I. Computation of electrical double layer properties in simple electrolytes. *J. Colloid Interf. Sci.* **63**, 480–499.

Davis J. A. and Leckie J. O. (1978b) Surface ionization and complexation at the oxide/water interface. II. Surface properties of amorphous iron oxyhydroxide and adsorption of metal ions. *J. Colloid Interf. Sci.* **67**, 90–105.

Dixit S. and Hering J. G. (2003) Comparison of arsenic(V) and arsenic(III) sorption onto iron oxide minerals: implications for arsenic mobility. *Environ. Sci. Technol.* **37**(18), 4182–4189.

Dixit S. and Hering J. G. (2006) Sorption of Fe(II) and As(III) on goethite in single- and dual-sorbate systems. *Chem. Geol.* **228**(1-3), 6–15.

Emmenegger L., King D. W., Sigg L. and Sulzberger B. (1998) Oxidation kinetics of Fe(II) in a eutrophic Swiss lake. *Environ. Sci. Technol.* **32**(19), 2990–2996.

Fenter P. and Sturchio N. C. (2004) Mineral–water interfacial structures revealed by synchrotron X-ray scattering. *Prog. Surf. Sci.* **77**, 171–258.

Fitts J. P., Machesky M. L., Wesolowski D. J., Shang X. M., Kubicki J. D., Flynn G. W., Heinz T. F. and Eisenthal K. B. (2005) Second-harmonic generation and theoretical studies of protonation at the water/alpha–TiO_2 (1 1 0) interface. *Chem. Phys. Lett.* **411**(4–6), 399–403.

Gaboriaud F. and Ehrhardt J. (2003) Effects of different crystal faces on the surface charge of colloidal goethite (alpha-FeOOH) particles: an experimental and modeling study. *Geochim. Cosmochim. Acta* **67**(5), 967–983.

Gehin A., Greneche J. M., Tournassat C., Brendle J., Rancourt D. G. and Charlet L. (2007) Reversible surface-sorption-induced electron-transfer oxidation of Fe(II) at reactive sites on a synthetic clay mineral. *Geochim. Cosmochim. Acta* **71**(4), 863–876.

Grahame D. C. (1947) The electrical double layer and the theory of electrocapillarity. *Chem. Rev.* **41**, 441–501.

Hansel C. M., Benner S. G. and Fendorf S. (2005) Competing Fe(II)-induced mineralization pathways of ferrihydrite. *Environ. Sci. Technol.* **39**(18), 7147–7153.

Hiemstra T., Barnett M. O. and van Riemsdijk W. H. (2007) Interaction of silicic acid with goethite. *J. Colloid Interf. Sci.* **310**, 8–17.

Hiemstra T., De Wit J. C. M. and van Riemsdijk W. H. (1989b) Multisite proton adsorption modeling at the solid/solution interface of (hydr)oxides: A new approach. II. Application to various important (hydr)oxides. *J. Colloid Interf. Sci.* **133**, 105–117.

Hiemstra T., Yong Ha and van Riemsdijk W. H. (1999b) Interfacial charging phenomena of aluminum (hydr)oxides. *Langmuir* **15**, 5942–5955.

Hiemstra T., Rahnemaie R. and van Riemsdijk W. H. (2004) Surface complexation of carbonate on goethite: IR spectroscopy, structure and charge distribution. *J. Colloid Interf. Sci.* **278**, 282–290.

Hiemstra T. and van Riemsdijk W. H. (1996a) A surface structural approach to ion adsorption: the charge distribution (CD) model. *J. Colloid Interf. Sci.* **179**, 488–508.

Hiemstra T. and van Riemsdijk W. H. (2002) On the relationship between surface structure and ion complexation of oxide–solution interfaces. In *Encyclopaedia of Surface and Colloid Science*. Marcel Dekker, Inc, New York, pp. 3773–3799.

Hiemstra T. and van Riemsdijk W. H. (2006) On the relationship between charge distribution, surface hydration and the structure of the interface of metal hydroxides. *J. Colloid Interf. Sci.* **301**, 1–18.

Hiemstra T., van Riemsdijk W. H. and Bolt G. H. (1989a) Multisite proton adsorption modeling at the solid/solution interface of (hydr)oxides: a new approach. I. Model description and evaluation of intrinsic reaction constants. *J. Colloid Interf. Sci.* **133**, 91–104.

Hiemstra T., Venema P. and van Riemsdijk W. H. (1996b) Intrinsic proton affinity of reactive surface groups of metal (hydr)oxides: the bond valence principle. *J. Colloid Interf. Sci.* **184**, 680–692.

Israelachvili J. N. and Wennerstrom H. (1996) Role of hydration and water structure in biological and colloidal interactions. *Nature* **379**(6562), 219–225.

Jeon B. H., Dempsey B. A. and Burgos W. D. (2003) Kinetics and mechanisms for reactions of Fe(II) with iron(III) oxides. *Environ. Sci. Technol.* **37**(15), 3309–3315.

Jing C. Y., Meng X. G., Liu S. Q., Baidas S., Patraju R., Christodoulatos C. and Korfiatis G. P. (2005) Surface complexation of organic arsenic on nanocrystalline titanium oxide. *J. Colloid Interf. Sci.* **290**(1), 14–21.

Kataoka S., Gurau M. C., Albertorio F., Holden M. A., Lim S. M., Yang R. D. and Cremer P. S. (2004) Investigation of water structure at the TiO_2/aqueous interface. *Langmuir* **20**(5), 1662–1666.

Keizer M. G. and van Riemsdijk W. H. (1998) ECOSAT, Technical Report Department Soil Science and Plant Nutrition. Wageningen Agricultural University.

Kim C. S., Rytuba J. J. and Brown G. E. J. (2004) EXAFS study of mercury(II) sorption to Fe- and Al-(hydr)oxides. I. Effect of pH. *J. Colloid Interf. Sci.* **271**, 1–15.

King D. W. (1998) Role of carbonate speciation on the oxidation rate of Fe(II) in aquatic systems. *Environ. Sci. Technol.* **32**(19), 2997–3003.

Kinniburgh D. G. (1993) Fit, Technical Report WD/93/23. British Geological Survey.

Klausen J., Trober S. P., Haderlein S. B. and Schwarzenbach R. P. (1995) Reduction of substituted nitrobenzenes by Fe(II) in aqueous mineral suspensions. *Environ. Sci. Technol.* **29**(9), 2396–2404.

Klebanov A. V., Bogdanova N. F., Ermakova L. E., Sidorova M. P. and Osmolovskii M. G. (2001) Electrosurface properties of hydr(oxides) and oxide nanostructures in 1:1 electrolyte solutions: 1. Adsorption characteristics of boehmite, goethite, and silicon dioxide. *Colloid J.* **63**(5), 562–567.

Klupinski T. P., Chin Y. P. and Traina S. J. (2004) Abiotic degradation of pentachloronitrobenzene by Fe(II): reactions on goethite and iron oxide nanoparticles. *Environ. Sci. Technol.* **38**(16), 4353–4360.

Larese-Casanova P. and Scherer M. M. (2007) Fe(II) sorption on hematite: New insights based on spectroscopic measurements. *Environ. Sci. Technol.* **41**(2), 471–477.

Lewis D. G. and Farmer V. C. (1986) Infrared Absorption of surface hydroxyl groups and lattice vibrations in Lepidocrocite (γ-FeOOH) and Boehmite (γ-AlOOH). *Clay Minerals* **21**, 93–100.

Liger E., Charlet L. and Van Cappellen P. (1999) Surface catalysis of uranium(VI) reduction by iron(II). *Geochim. Cosmochim. Acta* **63**(19-20), 2939–2955.

Lövgren L., Sjöberg S. and Schindler P. W. (1990) Acid/base reactions and aluminium (III) complexation at the surface of goethite. *Geochim. Cosmochim. Acta* **54**, 1301–1306.

Machesky M. L., Wesolowski D. J., Palmer D. A. and Ichiro-Hayashi K. (1998) Potentiometric titrations of rutile suspensions to 250 °C. *J. Colloid Interf. Sci.* **200**, 298–309.

Machesky M. L., Wesolowski D. J., Palmer D. A. and Ridley M. K. (2001) On the temperature dependence of intrinsic surface protonation equilibrium constants: an extension of the revised MUSIC model. *J. Colloid Interf. Sci.* **239**(2), 314–327.

Madrid L. and Diazbarrientos E. (1988) Description of titration curves of mixed materials with variable and permanent surface-charge by a mathematical-model .1. Theory. 2. Application to mixtures of lepidocrocite and montmorillonite. *J. Soil Sci.* **39**(2), 215–225.

Maithreepala R. A. and Doong R. A. (2004) Synergistic effect of copper ion on the reductive dechlorination of carbon tetrachloride by surface-bound Fe(II) associated with goethite. *Environ. Sci. Technol.* **38**(1), 260–268.

Manceau A., Nagy K. L., Spadini L. and Ragnarsdottir K. V. (2000) Influence of anionic structure of Fe–Oxyhydroxides on the structure of Cd surface complexes. *J. Colloid Interf. Sci.* **228**, 306–316.

Marcus Y. (1983) Ionic-radii in aqueous-solutions. *J. Solution Chem.* **12**(4), 271–275.

Nano G. V. and Strathmann T. J. (2006) Ferrous iron sorption by hydrous metal oxides. *J. Colloid Interf. Sci.* **297**(2), 443–454.

Nordin J., Persson P., Laiti E. and Sjoberg S. (1997) Adsorption of *o*-phthalate at the water-boehmite (gamma-AlOOH) interface: evidence for two coordination modes. *Langmuir* **13**(15), 4085–4093.

Ona-Nguema G., Morin G., Juillot F., Calas G. and Brown G. E. (2005) EXAFS analysis of arsenite adsorption onto two-line ferrihydrite, hematite, goethite, and lepidocrocite. *Environ. Sci. Technol* **39**(23), 9147–9155.

Ostroverkhov V., Waychunas G. A. and Shen Y. R. (2005) New information on water interfacial structure revealed by phase-sensitive surface spectroscopy. *Phys. Rev. Lett.* **94**(4), 1–4 (Art. No. 046102).

Parkman R. H., Charnock J. M., Bryan N. D. and Vaughan D. J. (1999) Reactions of copper and cadmium ions in aqueous solution with goethite, lepidocrocite, mackinawite, and pyrite. *Am. Miner.* **84**, 407–419.

Pashley R. M. and Israelachvili J. N. (1984) Molecular layering of water in thin films between mica surfaces and its relation to hydration forces. *J. Colloid Interf. Sci.* **101**(2), 511–523.

Pauling L. (1929) The principles determining the structure of complex ionic crystals. *J. Am. Chem. Soc.* **51**, 1010–1026.

Peacock C. L. and Sherman D. M. (2004) Copper(II) sorption onto goethite, hematite and lepidocrocite: a surface complexation model based on ab initio molecular geometries and EXAFS. *Geochim. Cosmochim. Acta* **68**(12), 2623–2637.

Pecher K., Haderlein S. B. and Schwarzenbach R. P. (2002) Reduction of polyhalogenated methanes by surface-bound Fe(II) in aqueous suspensions of iron oxides. *Environ. Sci. Technol.* **36**(8), 1734–1741.

Pedersen H. D., Postma D., Jakobsen R. and Larsen O. (2005) Fast transformation of iron oxyhydroxides by the catalytic action of aqueous Fe(II). *Geochim. Cosmochim. Acta* **69**(16), 3967–3977.

Persson P., Zivkovic K. and Sjoberg S. (2006) Quantitative adsorption and local structures of Gallium(III) at the water–alpha-FeOOH interface. *Langmuir* **22**(5), 2096–2104.

Rahnemaie R., Hiemstra T. and van Riemsdijk W. H. (2006) A new structural approach for outersphere complexation, tracing the location of electrolyte ions. *J. Colloid Interf. Sci.* **293**, 312–321.

Rahnemaie R., Hiemstra T. and van Riemsdijk W. H. (2007) Geometry, charge distribution and surface speciation of phosphate on goethite. *Langmuir* **23**, 3680–3689.

Randall S. R., Sherman D. M. and Ragnarsdottir K. V. (1999) The mechanism of cadmium surface complexation on iron oxyhydroxide minerals. *Geochim. Cosmochim. Acta* **63**, 2971–2987.

Randall S. R., Sherman D. M. and Ragnarsdottir K. V. (2001) Sorption of As(V) on green rust ($Fe_4(II)Fe_2(III)(OH)_{12}SO_4{\cdot}3H_2O$) and lepidocrocite (gamma-FeOOH): surface complexes from EXAFS spectroscopy. *Geochim. Cosmochim. Acta* **65**(7), 1015–1023.

Regazzoni A. E., Mandelbaum P., Matsuyoshi M., Schiller S., Bilmes S. A. and Blesa M. A. (1998) Adsorption and photooxidation of salicylic acid on titanium dioxide: a surface complexation description. *Langmuir* **14**(4), 868–874.

Ridley M. K., Machesky M. L., Wesolowski D. J. and Palmer D. A. (2004) Modeling the surface complexation of calcium at the rutile–water interface to 250 degrees C. *Geochim. Cosmochim. Acta* **68**(2), 239–251.

Rietra R. P. J. J., Hiemstra T. and van Riemsdijk W. H. (1999a) The relationship between molecular structure and ion adsorption on variable charge minerals. *Geochim. Cosmochim. Acta* **63**(19/20), 3009–3015.

Rietra R. P. J. J., Hiemstra T. and van Riemsdijk W. H. (2000a) Electrolyte anion affinity and its effect on oxyanion adsorption on goethite. *J. Colloid Interf. Sci.* **229**, 199–206.

Rodriguez R., Blesa M. A. and Regazzoni A. E. (1996) Surface complexation at the TiO_2 (anatase) aqueous solution interface: chemisorption of catechol. *J. Colloid Interf. Sci.* **177**(1), 122–131.

Rustad J. R., Felmy A. R. and Hay B. P. (1996b) Molecular statics calculations of proton binding to goethite surfaces: a new approach to estimation of stability constants for multisite surface complexation models. *Geochim. Cosmochim. Acta* **60**, 1563–1576.

Shen Y. R. and Ostroverkhov V. (2006) Sum-frequency vibrational spectroscopy on water interfaces: Polar orientation of water molecules at interfaces. *Chem. Rev.* **106**(4), 1140–1154.

Silvester E., Charlet L., Tournassat C., Gehin A., Greneche J. M. and Liger E. (2005) Redox potential measurements and Mossbauer spectrometry of Fe-II adsorbed onto Fe-III (oxyhydr)oxides. *Geochim. Cosmochim. Acta* **69**(20), 4801–4815.

Spadini L., Manceau A., Schindler P. W. and Charlet L. (1994) Structure and stability of Cd^{2+} surface complexes on ferric oxides. 1 Results from EXAFS spectroscopy. *J. Colloid Interf. Sci.* **168**, 73–86.

Spadini L., Schindler P. W., Charlet L., Manceau A. and Ragnarsdottir K. V. (2003) Hydrous ferric oxide: evaluation of CD-HFO surface complexation models combining Cdk EXAFS data, potentiometric titration results and surface site structures identified from mineralogical knowledge. *J. Colloid Interf. Sci.* **266**, 1–18.

Spadini L., Schindler P. W. and Sjoberg S. (2005) On the stability of the AlOSi(OH)(3)(2+) complex in aqueous solution. *Aquat. Geochem.* **11**(1), 21–31.

Stachowicz M., Hiemstra T. and van Riemsdijk W. H. (2006) Surface speciation of As(III) and As(V) adsorption in relation to charge distribution. *J. Colloid Interf. Sci.* **302**, 62–75.

Stern O. (1924) Zur theory der electrolytischen doppelschicht. *Z. Electrochem.* **30**, 508–516.

Strathmann T. J. and Myneni S. C. B. (2005) Effect of soil fulvic acid on nickel(II) sorption and bonding at the aqueous-boehmite (gamma-AlOOH) interface. *Environ. Sci. Technol.* **39**(11), 4027–4034.

Strathmann T. J. and Stone A. T. (2003) Mineral surface catalysis of reactions between Fe-II and oxime carbamate pesticides. *Geochim. Cosmochim. Acta* **67**(15), 2775–2791.

Stumm W. and Sulzberger B. (1992) The cycling of iron in natural environments—considerations based on laboratory studies of heterogeneous redox processes. *Geochim. Cosmochim. Acta* **56**(8), 3233–3257.

Sun X. and Doner H. (1996) An Investigation of Arsenate and Arsenite Bonding Structures on Goethite by FTIR. *Soil Sci.* **161**, 865–872.

Sverjensky D. A. (2005) Prediction of surface charge on oxides in salt solutions: revisions for 1:1 (M + L−) electrolytes. *Geochim. Cosmochim. Acta* **69**(2), 225–257.

Tamura H., Goto K. and Nagayama M. (1976) Effect of ferric hydroxide on oxygenation of ferrous-ions in neutral solutions. *Corrosion Sci.* **16**(4), 197–207.

Toney M. F., Howard J. N., Richer J., Borges G. L., Gordon J. G., Melroy O. R., Wiesler D. G., Yee D. and Sorensen L. B. (1995) Distribution of water molecules at Ag(111)/electrolyte interface as studied with surface X-ray scattering. *Surf. Sci.* **335**(1–3), 326–332.

Venema P., Hiemstra T. and van Riemsdijk W. H. (1998) Intrinsic proton affinity of reactive surface groups of metal (hydr)oxides: application to iron (hydr) oxides. *J. Colloid Interf. Sci.* **198**, 282–295.

Vikesland P. J. and Valentine R. L. (2002a) Iron oxide surface-catalyzed oxidation of ferrous iron by monochloramine: implications of oxide type and carbonate on reactivity. *Environ. Sci. Technol.* **36**(3), 512–519.

Vikesland P. J. and Valentine R. L. (2002b) Modeling the kinetics of ferrous iron oxidation by monochloramine. *Environ. Sci. Technol.* **36**(4), 662–668.

Waychunas G. A., Fuller C. C. and Davids J. A. (2002) Surface complexation and precipitate geometry for aqueous Zn(II) sorption on ferrihydrite I: X-ray absorption extended fine structure spectroscopic analysis. *Geochim. Cosmochim. Acta* **66**(7), 1119–1137.

Waychunas G. A., Rea B. A., Fuller C. C. and Davids J. A. (1993) Surface chemistry of ferrihydrite. 1. EXAFS studies of the geometry of coprecipitated and adsorbed arsenate. *Geochim. Cosmochim. Acta* **57**, 2251–2269.

Wehrli B. and Stumm W. (1989) Vanadyl in natural-waters—adsorption and hydrolysis promote oxygenation. *Geochim. Cosmochim. Acta* **53**(1), 69–77.

Wehrli B., Sulzberger B. and Stumm W. (1989) Redox processes catalyzed by hydrous oxide surfaces. *Chem. Geol.* **78**(3–4), 167–179.

Weidler P. G. (1996) *Oberflächen und porositäten synthetischer Eisenoxide*. Technische Universität München, Munchen.

Weidler P. G., Hug S. J., Wetche T. P. and Hiemstra T. (1999) Determination of growth rates of 100 and 110 faces of synthetic goethite by scanning force microscopy. *Geochim. Cosmochim. Acta* **62**, 3407–3412.

Westall J. and Hohl H. (1980) A comparison of electrostatic models for the oxide/solution interface. *Adv. Colloid Interf. Sci.* **12**, 265–294.

Williams A. G. B. and Scherer M. M. (2004) Spectroscopic evidence for Fe(II)–Fe(III) electron transfer at the iron oxide–water interface. *Environ. Sci. Technol.* **38**(18), 4782–4790.

Yates D. E., Levine S. and Healy T. W. (1974) Site-binding model of the electrical double layer at the oxide/water interface. *J. Chem. Soc. Faraday Trans. I* **70**, 1807–1818.

Yeganeh M. S., Dougal S. M. and Pink H. S. (1999) Vibrational spectroscopy of water at liquid / solid interfaces: crossing the isoelectric point of a solid surface. *Phys. Rev. Lett.* **83**(6), 1179–1182.

Zachara J. M., Smith S. C. and Fredrickson J. K. (2000) The effect of biogenic Fe(II) on the stability and sorption of $Co(II)EDTA^{2-}$ to goethite and subsurface sediment. *Geochim. Cosmochim. Acta* **64**(8), 1345–1362.

Zhang Y., Charlet L. and Schindler P. W. (1992) Adsorption of protons, Fe(II) and Al(III) on lepidocrocite (Gamma-FeOOH). *Colloids Surf.* **63**(3–4), 259–268.

Zhang Z., Fenter P., Cheng L., Sturchio N. C., Bedzyk M. J., Predota M., Bandura A., Kubicki J. D., Lvov S. N., Cummings P. T., Chialvo A. A., Ridley M. K., Benezeth P., Anovitz L., Palmer D. A., Machesky M. and Wesolowski D. J. (2004) Ion adsorption at the rutile–water interface: linking molecular and macroscopic properties. *Langmuir* **20**(12), 4954–4969.

Zhang Z., Fenter P., Kelly S. D., Catalano J. G., Bandura A. V., Kubicki J. D., Sofo J. O., Wesolowski D. J., Machesky M. L., Sturchio N. C. and Bedzyk M. J. (2006) Structure of hydrated Zn^{2+} at the rutile TiO2 (110)-aqueous solution interface: comparison of X-ray standing wave, X-ray absorption spectroscopy, and density functional theory results. *Geochim. Cosmochim. Acta* **70**(16), 4039–4056.

Zhukhlistov A. P. (2001) Crystal structure of lepidocrocite Fe O (O H) from electron diffraction data. *Kristallografiya* **46**(5), 805–808.

Associate editor: Michael L. Machesky